Doctoral Dissertation(Shinshu University)

Synthesis of porous coordination polymers comprising Zn^{2+}, triazole, and oxalic acid under magnetic fields and their adsorptivity for carbon dioxide

March 2017

By

MOONDRA ZUBIR

Submitted to

SHINSHU UNIVERSITY

DEPARTMENT OF MATERIAL SCIENCE AND ENGINEERING
INTERDISCIPLINARY GRADUATE SCHOOL OF SCIENCE AND TECHNOLOGY
SHINSHU UNIVERSITY
JAPAN

CONTENTS

FIGURES

TABLES

ABBREVIATIONS

PCPs	- porous coordination polymers
MOFs	- metal organic frameworks
1D	- One dimensional
2D	- Two dimensional
3D	- Three dimensional
Taz	- 1,2,4-triazole
ATaz	- 3-amino, 1,2,4-triazole
Oxac	- oxalic acid
ZOTW	- zinc oxalic acid triazole water
ZOT	- zinc oxalic acid triazole
MIL	- material institute lavoiser
LPC	- latent porous complex
CPL	- coordination pillared layer
PCN	- porous coordination network
IRMOF	- isoreticular metal organic frameworks
ZIF	- zeolite imidazolate frameworks
ELM	- elastic layer-structured metal organic frameworks
TCNQ	- 7,7,8,8-Tetracyanoquinodimethane
Bdc	- bi-dicarboxylic acid
Bpy	- 4,4`-bipyridin
XRD	- X-ray diffraction
SEM	- scanning electron microscope
TGA	- thermo gravimetric analysis
DTA	- differential thermal analysis
EDS	- energy dispersive x-ray spectroscopy

Chapter 1 Introduction

1.1. Porous materials

Porous materials are of great advantage to application in environmental and energy problems, such as catalysts, adsorbents, sensors, insulators, etc. Properties of porous material depend on the pore structure of each material. Some porous solids exists as agglomerates which are relatively rigid, macroscopic particles whose dimensions exceed those of the pores by many orders of magnitude. Others are being non rigid, more or less loosely packed assemblages of individual particles which referred to as aggregates.

Pores also can be classified by their connectivity in a particle as shown in Figure 1 [1]. The pores accessible to the external surface are named open pores like b, c, d, e and f. They are accessible for molecules or ions in the surrounding. Some may be open at two ends (e) and the others only at one end (b and f) which are called ink-bottle pore (b) and blind (dead-end) pore (f). Ink-bottle pore is relatively large-volume pore that is connected to the surface or other open porosity through a narrow constriction or throat [2].

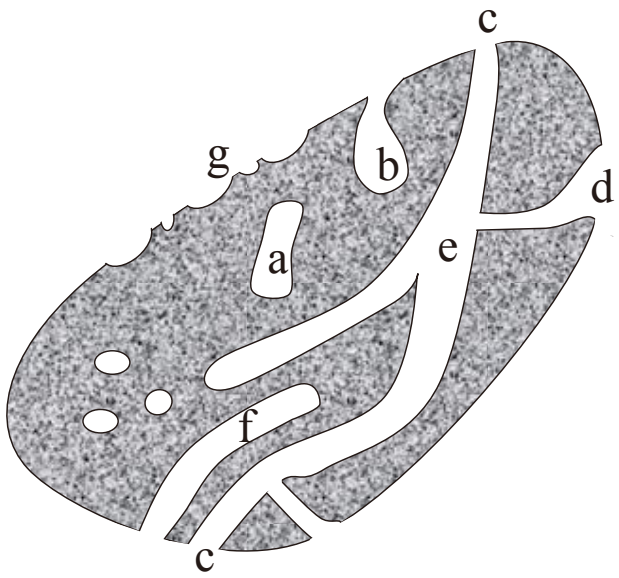

Figure 1. Schematic pores classification, according to their availability to surrounding. a, closed pores; b and f, pores open only at the end; c,d, and g, open pores; e, open at two ends (through) pores [1].

Blind or dead-end pore is open at one end only and can be accessed fully to the surface, though their way in transport is often negligible. Shallow dead-end pores are in some cases called surface roughness [2]. When the porous solids are heated, the entrance of pores sometimes collapse to lead to closed pores. The closed pore is not associated with adsorption and permeability of molecules, but it influences the mechanical properties of solid materials [1].

Closed pore is the pores that cannot be penetrated by He at 303 K. The other interpretation of closed pore is an open pore whose width is smaller than molecular size of probe molecules. Some of closed pores are the latent pores which can certain conditions. There are various kinds of pores in sizes described in the literature that is summarized in Table 1.

Table 1. Summary of the most frequently used pore size classifications [1].

Classification	Specified types of pores, d(nm) and the range of diameters					
	Macro-	Meso-	Micro-	Super micro-	Ultra micro-	Sub micro-
IUPAC	d > 50	2 - 50	d < 2 (0.4 - 2)	0.7 - 2	d < 0.7	d < 0.4
Dubinin	200 - 400	200-400 > d > 3 - 3.2	< 1.2 - 1.4	3 - 3.2 > d > 1.2 - 1.4	-	-
Cheremskoj	d > 2000	-	2000 > d > 200	-	d < 2 - 4	d < 200
Kodikara	10^4 - 10^6	-	10^3 - $3x10^4$	25 - 103	d < 3 - 4	-

Micropores and mesopores have an important role in the adsorption phenomena. Recently, the term nanopore has been used, which is less than 100 nm in diameter [1]. The pore volume is usually regarded as the volume of open pores, which should depend on the nature of the probe molecule and ~~or~~ the experimental conditions. The ratio of pore volume to total volume of the solid is defined as porosity [3].

No surface of any solid is smooth on an atomic level. There are present cracks and fissures, some of which may penetrate very deeply to make internal surfaces. It is difficult to distinguish between roughness and porosity [1]. Despite its arbitrariness the distinction between an external and an internal surface is useful in practice: a wide range

of porous solids has an internal surface greater by several orders of magnitude than the external surface, the total surface of the solid thus being predominantly internal. Very fine powders of numerous substances, on the other hand, have a large and small or even negligible, internal surface. When aggregation of such particles occurs, for reasons already referred to, then part of the external surface becomes converted into an internal surface and a pore system is developed.

The structures of pore can be designed from various view points. PCPs are investigated as porous crystalline solids such as zeolites and clays. These pores are generally of molecular dimensions and are arranged as highly regular networks. The second type of porous material is composed of an assemblage of small particles. The pore structure of the consolidated system is mainly dependent on the size and packing density of the primary particles: the process is, therefore constitutive. A third route is subtractive since inherent parts of the original structure are removed to create the pores, for example, the thermal decomposition of a hydroxide or carbonate or a leaching process to produce porous glass [1].

1.2. Overview of porous coordination polymers (PCPs)

The porous compounds have attracted the attention of chemists, physicists and material scientist because of interest in the creation of nanometer-sized spaces and phenomena in them. There is also commercial interest in their application in separation, storage of materials, and heterogeneous catalysis. Recently, porous coordination polymers (PCPs) have been developed, which are beyond the scope of the former two classes of porous materials; are inorganic and carbon based materials. Microporous coordination polymers have perfectly regular pores as found in zeolites and high porosity as found in carbon based materials. The structural integrity of the building units is maintained throughout the reactions which allow their use as modules in the assembly of extended structures.

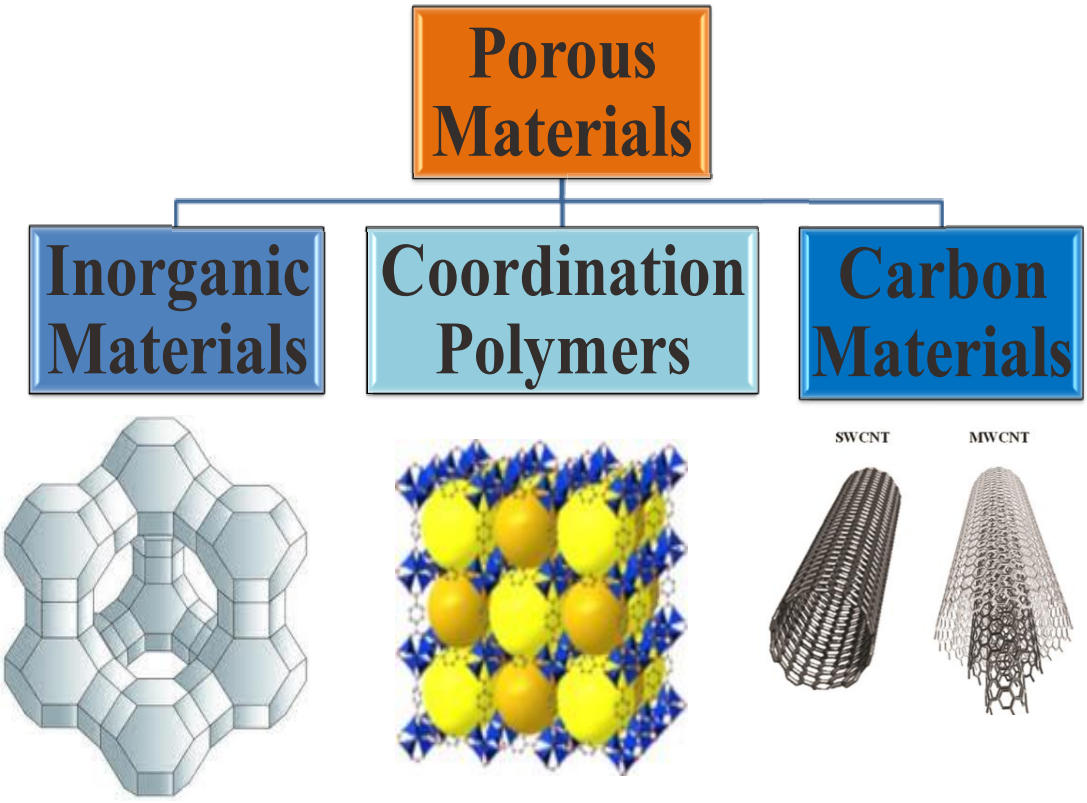

Figure 2. Classification of porous materials

Coordination polymers are highly crystalline materials and need good quality single crystals to understand their structure and properties. Porous coordination polymer synthesis is carried out under mild conditions and the choice of a certain combination of multi-components to desire extended network. Their structures are based on metal center as the connectors and organic ligands as linkers. The majority of metal ion/metal clusters are transition metals with various geometries, due to their versatile coordination numbers. These geometries include square-planar, tetrahedron and octahedron among others.

Transition-metal ions are often utilized as versatile connectors in the construction of coordination polymers. Depending on the kind of metal and its oxidation state, the coordination number can range from 2 to 7, which gives rise to various geometries as the following schemes [7].

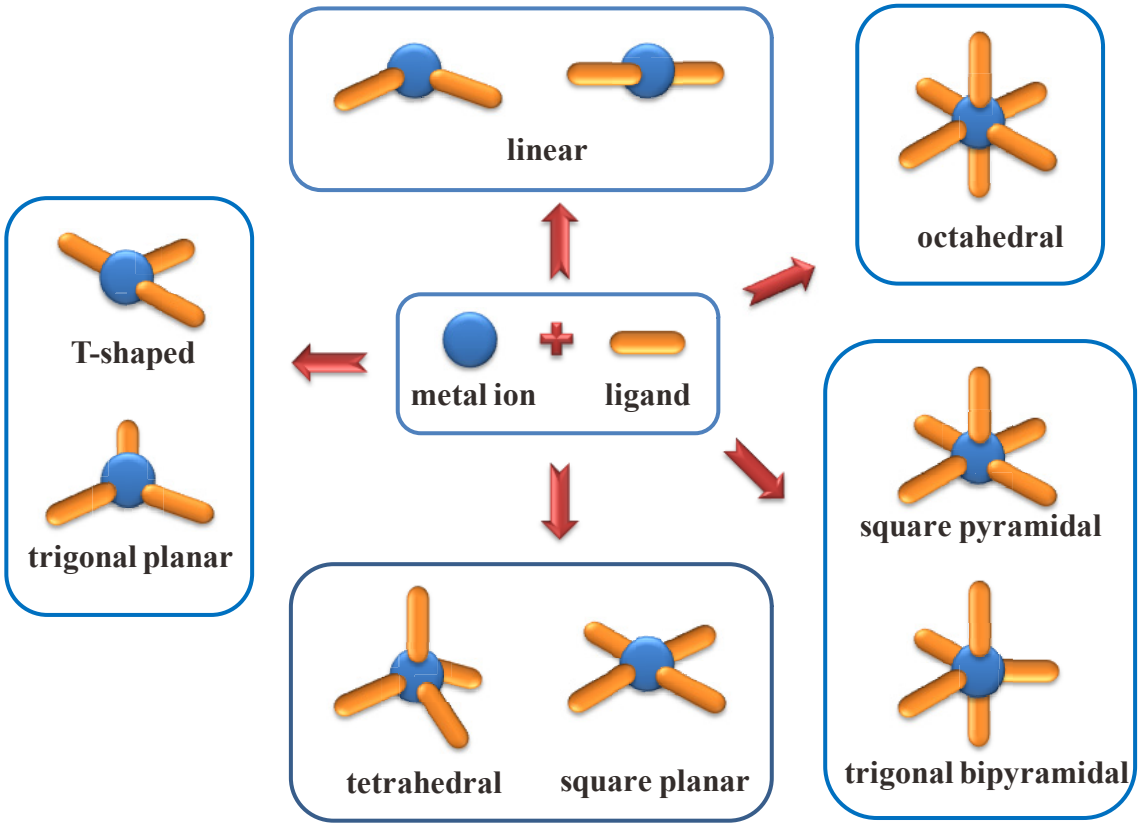

Figure 3. Coordination geometries of transition metal ions [7].

The rich functionality and design of organic ligands and physical properties of the metal ions are fascinating for the design of various functions, such as not only adsorptive functions such as storage, separation, and catalysis, but also other chemical/physical functions that can be integrated in the frameworks. PCPs can be tuned and designed systematically based on changing the nature of organic linkers and changing the connectivity of the inorganic moiety, and how the building blocks come together to form a network. Linkers afford a wide variety of linking sites with tuned binding strength and directionality. Halides (F^-, Cl^-, Br^-, and I^-) are the smallest and simplest in all linkers beside more complexes organic linker ligand as neutral, anionic, and cationic organic ligands, [7], as described below:

1. Neutral organic ligands

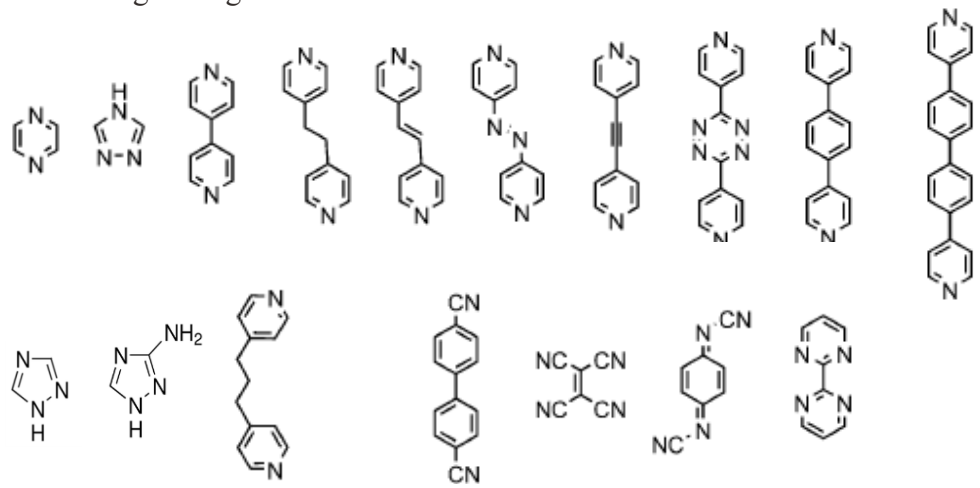

2. Anionic organic ligands

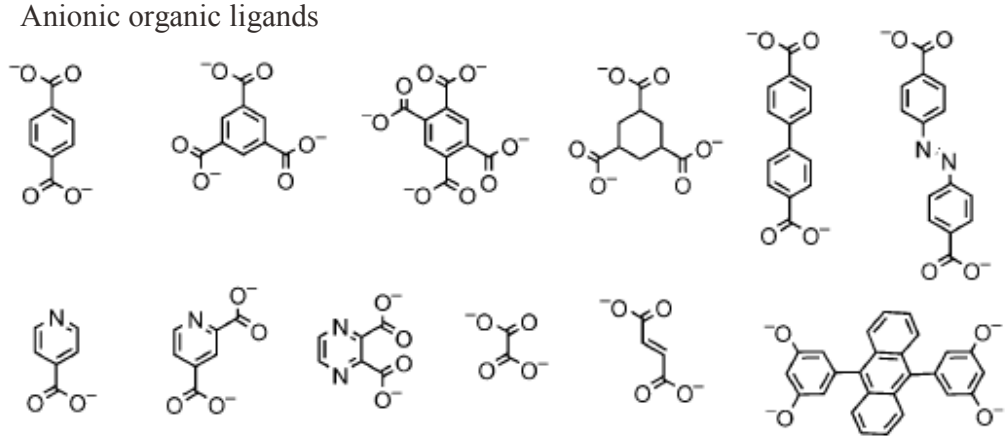

3. Cationic organic ligands

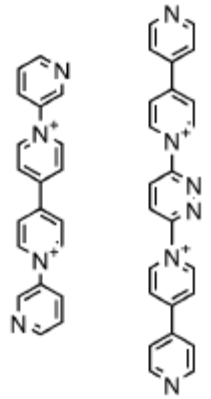

Figure 4. Examples of linkers used in coordination polymers [7].

This remarkable and easy tunability of PCPs are a key feature that distinguishes these materials from traditional porous materials, such as zeolites and activated carbons. The components of PCPs are connected by coordination bonds with weak interactions and non-covalent bonds (H-bonds, π-electron stacking, and van der Waals interactions). The interactions lead to structural flexibility and dynamics properties in the crystalline state, which also promotes the unique character of PCPs in the field of porous materials. Furthermore, designing pore structure and propertiey, it is possible to modify the pores which interact with specific molecules [8].

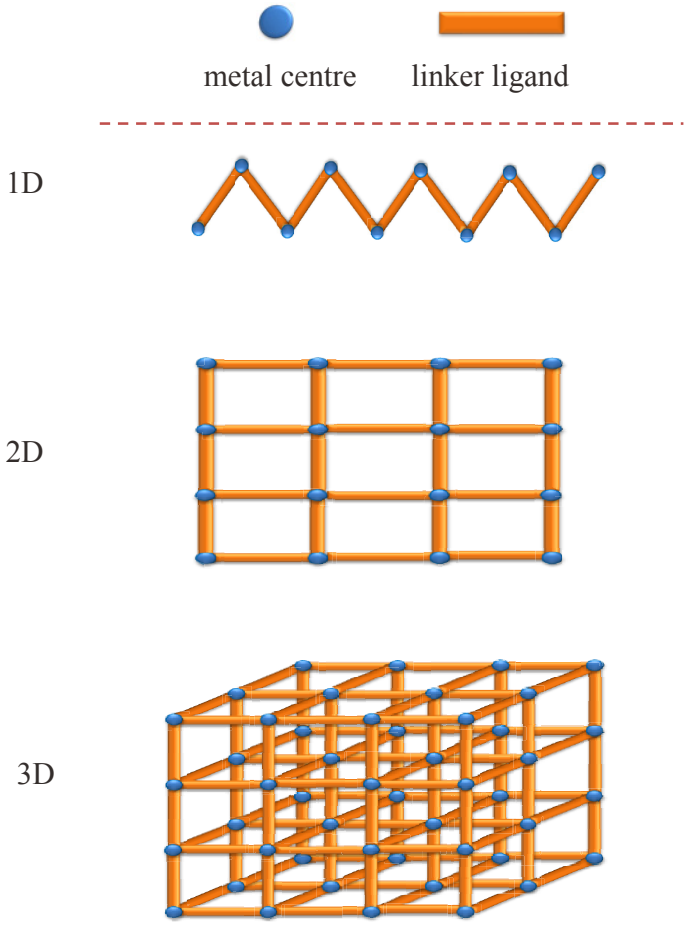

Figure 5. Coordination polymer networks [7].; 1D, 1-dimensional;; 2D, 2-dimensional; 3D, 3-dimentional [7]..

1.3. Design of functional porous coordination polymers.

PCP materials consist of three dimensional organic-inorganic hybrid networks, formed by metal based nodes (e.g. Al^{3+}, Cr^{3+}, Cu^{2+}, or Zn^{2+}) bridged by organic linker groups (e.g. carboxylate, pyridyl). Due to strong coordination bonds, the framework structures of PCPs are geometrically and crystallographically well defined [9].

Similar to the synthesis of organic copolymers, the building blocks of PCPs are carefully chosen because their properties are retained and exhibited by the products. Whereas the nature and number of monomers in an organic polymer determine its process ability and physical characteristics, it is the network connectivity of the building units that largely determines the properties of PCPs. Consequently, PCPs synthesis requires not only the selection or preparation of desired modules, but also some foresight as to how they will be assembled in the final solid [10].

The first coordination polymer, $Ni(CN)_2(NH_3)\cdot C_6H_6$, was synthesized by Hofmann and Kuspert in 1897 [11], called Hofmann Complex. The coordination polymer was formed by reacting slowly C_6H_6 with $Ni(CN)_2$ in an NH_3 solution. The structure of coordination polymers was later refined using X-ray crystallography, as a two-dimensional layer structure formed by covalent linkages between Ni and CN groups [12]. The parallel layers are held up by extruding NH_3 groups, and forming inter-planar cavities in which benzene molecules reside. The work inspired research towards designing various inorganic-organic hybrid polymers using diamines, such as 4,4'-bipyridine.

1.3.1. Principles in synthesis of PCPs

A large number of new PCPs have emerged ~~in~~ for the last ~~few years~~ two decades. However, their methods of preparation are quite similar. In most ~~of the~~ resulting materials, the solvent used for synthesis is removed by degassing, heating, or exchange with volatile molecules, and large pore volume and surface area accessible to guest molecules are formed. The self assembly process for coordination polymers is a useful ~~method~~ rout for the following reasons [13]:

- A wide variety of frameworks can be realized just from simple building blocks of metal ions, organic ligands, and counter anion.

- Easy and rational modification of organic bridging ligands is possible.
- Several interactions such as coordination bonds, hydrogen bonds, aromatic interaction, and van der Waals interaction are available.
- The reaction can be controlled by temperature, pH, solvent, pressure, etc.

Several factors must be borne in mind in approaching to the synthesis of new PCPs, aside from the geometric principles that are considered during its design. The most important thing is the maintenance of the integrity of the building blocks. A great deal of effort has been quite often expended on the synthesis of a novel organic linker and reaction conditions must be mild enough to maintain the functionality and conformation of this moiety, which should be reactive enough to establish the metal-organic bonds [10]. The following parameters can play a key role in PCPs optimization and synthesis:

- Temperature
- Solvent composition
- Reaction time
- Reagent ratio
- Reagent fraction.

There are several synthesis approaches for PCPs.

1. Diffusion method

Rapid mixing of a solution containing metal ions and a solution containing bridging ligands affords microcrystals powder with a size of the order of μm. Because of this small size, such powder samples are not suitable for single crystal XRD analysis. To avoid precipitation of powders, a diffusion method is frequently used [13].

2. Solvothermal method

The solvothermal method, which is well established for the synthesis of zeolites, has been advanced for coordination polymers. This reaction is typically carried out in the temperature range of 390-530 K under autogenous pressure, and exploits the self-assembly of the product from soluble precursors. The reduced viscosity of water under this condition enhances the diffusion processes so that solvent extraction of solids and crystal growth from solutions are favored. Because the problems of difference in solubility are minimized, a variety of simple precursors may be introduced, as well as a number of organic and/or inorganic structure-directing agents [13].

Solvothermal technique is widely applied to synthesize novel metal oxides from reaction mixture inside a closed reaction vessel, under the supercritical temperature of the solvent of either aqueous or organic liquid [14,15]. Compared with other synthesis methods such as ceramic, sol-gel techniques, the main advantages of the solvothermal techniques are:

a. Simple one-pot/one-step preparation/synthesis;
b. Ability to control the morphology of material crystals.
c. Efficient synthesis conditions, with milder synthesis temperature and shorter synthesis duration, possibly due to reduced viscosity and dielectric constants [16].

3. Solvent-free method

Solvent-free synthesis is of interest for several reasons. It could give insight into the roles of solvent molecules in templating microporous structures, give access to large scale green production process, and even provides more convenient lab-scale preparative methods. This solvent-free method is quick and gives a quantitative yield, without solvents or external heating. Clearly, it can presents higher efficiency in terms of materials, energy, and time compared with solvothermal method [13].

4. Microwave and ultrasonic methods

Microwave irradiation has been developed as a novel heating technique for the solvothermal synthesis of organic or inorganic solid-state materials. In particular, this method has been shown to provide an efficient way to synthesize purely inorganic porous materials with short crystallization times, narrow particle size distributions, facile morphology control, phase selectivity, and efficient evaluation to process parameters [13].

The ultrasonic method is also expected to be useful, but few instances have been reported for coordination polymers. The weight-averaged molecular weight (M_w) of the coordination polymer is reversibly reduced upon irradiation of ultrasound for 1 h. Upon equilibration, the original molecular weight distribution is fully restored within 24h. The reversibility of the ultrasonic scission process indicates that only coordination bonds and no covalent bonds are broken [10].

1.3.2. Crystal structure of PCPs.

PCPs can be categorized into following four sub-sets: rigid frameworks, flexible/dynamic frameworks, surface functionalized frameworks, and open metal sites. Rigid framework PCPs usually have stable and robust porous frameworks with permanent porosity, which shows a normal type I shape adsorption isotherms.

Flexible PCPs show extreme changes in the framework when the guest molecules are inserted or removed, and are affected by external stimuli, such as pressure and temperature. Flexible PCPs exhibit stepwise and hysterestic adsorption isotherms for CO_2 and other gases. The surface functionalized frameworks enhance the capacity and selectivity of PCPs for guest molecules. For example, adsorption capacity for CO_2 is enhanced by grafting functional groups into the surface of pores, such as arylamine, alkylamine, and hydroxyl groups [8].

The fourth set of PCPs is open metal site frameworks. Open metal sites enhance PCPs in performance for the separation of polar/non polar gas mixture such as CO_2/CH_4. The most attractive phenomena due to open metal sites of PCPs is outstanding enhancements in their CO_2 capture ability in the presence of water in such frameworks [10].

1.3.3. Characterization of PCPs.

Various characterization techniques are employed for both single crystal and powders as detailed below.

1. Powder X-ray diffraction

Powder X-ray diffraction (XRD) is a technique used to characterize the crystallographic structure, crystallite size (grain size), and preferred orientation in polycrystalline or powdered solid samples. Powder diffraction is commonly used to identify unknown substances, by comparing diffraction data against a database maintained by the International Centre for Diffraction Data (ICDD) [17].

Figure 6 shows the basic features of an X-ray diffractometer, in which the diffraction angle 2θ is the angle between the incident and diffracted X-rays.

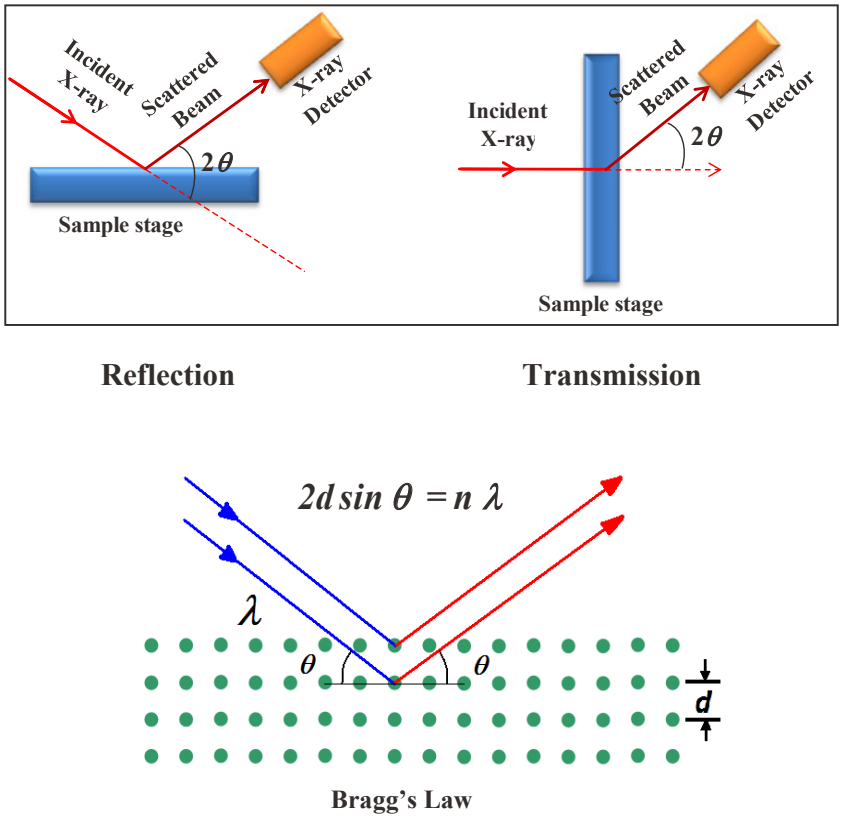

Figure 6. Basic features of an X-ray diffractometer [17]. *d,* spacing between layers in atoms; λ, the wavelength of the rays; *n*, order of diffraction (an integer); θ, the angle between the incident rays and the surface of the crystal.

The crystal structures of PCPs are, in general, unambiguously determined using crystallographic techniques such as X-ray diffraction, the availability of XRD is undoubtedly another factor contributing to the popularity of the PCPs field. However, although these techniques are widely employed and well understood (being over a century old), the structure solution of highly porous materials is not always a straightforward process. Factors which prevent trivial structural elucidation include the presence of a large amount of pore-occupying, disordered solvent molecules (sometimes resulting in refined structures with residual values larger than those typically reported for

molecular crystals), or difficulties associated with growing good diffraction-quality crystals. In addition, new techniques are being developed and applied to further study the fascinating properties of these materials, which in many cases require diffraction under non ambient conditions (i.e. high pressure, high temperature). Single-crystal X-ray diffraction is rightly considered the ultimate technique for the structural determination of crystalline materials. This is a very mature technique that has become readily accessible, and this accessibility is accompanied by vast improvements in the related instrumentation. When PCP single-crystal growth is not possible, structural solution from powder diffraction data can be accomplished. So far, several different standalone or combined approaches have been successfully employed to solve the crystal structure of PCPs using powder diffraction. The structural solution of PCPs without any previous information has been reported using the application of direct methods to powder data, notably in the case of UiO-66 [18], which was solved by direct methods implemented in the program EXPO using high quality data collected with synchrotron radiation. The process is not dissimilar to that carried out for any other type of material, with a typical approach involving the pattern indexing, intensity integration, structure solution and final Rietveld refinement. This same process can be carried out with the charge-flipping method [20] instead of direct methods, as in the case of another family of PCPs known as metal-triazolates (METs) [21]. The procedure to obtain the initial solution is equivalent to the one that would be followed by single crystal diffraction data, although includes modifications such as histogram matching with chemical composition [22]. Recently it has also been reported that the solution obtained with application of the charge-flipping method to powder diffraction data can be greatly improved, provided that an initial set of phases is obtained for at least low-resolution reflections. These initial sets are supplied to the input data so that they are not randomly assigned in the first step of the charge-flipping cycle. This set of phases can be obtained with the use of high-resolution electron microscopy [23], but most interestingly it has been recently demonstrated that they can also be obtained with the use of only powder X-ray diffraction (PXRD) data, by applying the charge-flipping method initially to only a few subsets of reflections corresponding to low-resolution two-dimensional projections [24]. The use of these phases obtained by method in the subsequent application of the charge-flipping method with the full data set

resulted in greatly improved electron density maps that could be interpreted, unveiling the structure of microporous zeolites. It can be anticipated that this same method can be applied to the structure solution of porous PCPs with only the use of powder diffraction data [25].

2. Optical Microscopy

Optical microscopy is perhaps the easiest to perform given the easy access of optical microscopes. This is most useful on single-crystals which exhibit a color change on metal or ligand exchange. A uniform color change occurring in a single crystal is strong evidence that exchange has occurred homogeneously and only a single domain is present [12].

3. SEM-EDS and TEM-EDS

Scanning electron microscopy is a technique in which a sample is imaged by exposing it to a high energy-beam of electrons and scanning this beam across the specimen. The use of Scanning Electron Microscopy/Energy Dispersive X-Ray Spectroscopy (SEM/EDS) is the analysis of failure some materials. Scanning Electron Microscopy (SEM) allows for visual observation of an area of interest in a completely different way from that of the naked eye or even normal optical microscopy. SEM images show simple contrasts between organic-based and metallic-based materials and thus instantly provide a great deal of information about the area being inspected. At the same time, Energy Dispersive X-Ray Spectroscopy (EDS), sometimes referred to as EDAX or EDX, can be used to obtain semi-quantitative elemental results about very specific locations within the area of interest [26].

SEM-EDS and TEM-EDS is a useful characterization technique for PCPs, especially for metallic elements. Energy dispersive X-ray maps of elements can be constructed to show that the distribution of metals in each PCP particle is identical and uniform if PCP are synthesized.

1.3.4. Modification in frameworks flexibility of PCPs

The variety of combinations of organic linkers and metal ions suggest the possibility of the creation of multifunctional porous frameworks, in which two or more physical/chemical properties are integrated in the crystal. For example, some PCPs have

guest-responsive magnetic activity in the framework, i.e., switching in magnetic properties by the insertion/release of guest molecules.

1. Porosity and magnetism

PCP magnets incorporating magnetic properties into the framework are unique multifunctional materials, particularly as chemo-responsive materials, because of the mutual interplay of porous functions and magnetic switching. Many reports on porous magnets using in PCP framework have appeared [27]; however, there are few examples that show a combination of porous and magnetic functions, because most porous magnets undergo a magnetic transformation at very low temperature (critical temperature), whereas the adsorptive functions occur at ambient temperature. On the other hand, spin crossover (SC), in which electron configurations can be switched between high and low spin states in response to external stimuli, producing changes in magnetism, color, and dielectric properties and structure, is often observed at ambient temperature. Thus, we could design a real interplay of SC phenomena and adsorption properties.

2. Porosity and conductivity/dielectricity

Incorporation of electric conductivity in the porous materials is widely regarded as a challenging task. A combination of porosity and electric conductivity is applicable for gas sensors, such as electrodes. Only limited numbers of conductive coordination polymers have been reported and the coexistence of permanent porosity is still rare. Multifunction porosity-dielectric properties have also been studied in recent years. For example, $Mn_3(HCOO)_6(C_2H_5OH)$ having 1 D channels occupied by ethanol as a guest shows a ferromagnetic transition at 8.5K due to the magnetic transition of the Mn^{2+} spin [28]. The dielectric constant of this framework is heavily dependent on the axis of the crystal and the specific axis of the guest ethanol which aligns in parallel. The temperatures of phase transition are attributed to reorientation of the guest molecules and it contributes to the ferroelectricity in the framework. The guest-induced ferroelectricity is unique for porous materials and the interplay among the porosity, magnetism, and ferroelectricity, in other words, porous materials with multi ferroic behavior are of great interest for multifunctional porous design [29-32].

3. Mixed ligand and mixed metals

In principle, PCP frameworks can be constructed from multiple organic ligands and metal ions. However, there are limited numbers of reports on frameworks having more than two kinds of ligands or metal ions. Considering that the doping approach has been popular in the area of inorganic materials such as metal oxides and metals, the on-demand doping of metal ions or organic ligands in the PCP frameworks should become another important strategy for multifunctional system.

The potential of the mixed-ligand approach in the framework of $Zn_4O(L)_3$ (L = terephthalic acid derivatives) was extended by the use of a high-throughput technique [33]. On the scaffold of the structure, various terephthalic acid derivatives can be incorporated to create a porous structure, and one of them has eight terephthalic acid derivatives in the crystal structure. The distribution of functional groups in the ligands is disordered and the adsorption property of some of the members of this series exhibits up to 400% better selectivity for CO_2 over CO compared with the best same-link counterparts. This also suggests that the matching of the interval of ligands and comparable strengths of coordination bonds are the key to integrating the different ligands in the structure, although each of them has different substituent groups. The reaction conditions should be optimized to synthesize mixed-ligand PCPs and powerful screening with the aid of robots is becoming important. The control of structural flexibility in the PCP has been a major challenge because a small difference in flexibility often contributes to the gas separation. The ligand doping approach for soft type PCPs is a significant one to regulate the flexibility.

Not only ligand mixing in the single structure, but also mixing of metal species have been reported. Co^{2+} doping to replace Zn^{2+} ions in the framework of $Zn_4O(bdc)_3$ has been reported [34]. Co^{2+} is coordinated to six oxygen atoms in the metallic cluster, two of which belong to diethylformamide molecules. The CoZn-MOF-5 materials prepared have higher adsorption capacities for H_2, CO_2, and CH_4 at high pressure than their Co-free homologs. Other well-known PCPs such as HKUST-1 and MIL-3 have also been prepared for doping of metal sites and their magnetic behavior and thermal stability have been studied [35, 36].

4. Changing the ligand length

A method to modify the adsorption properties is to change the length of the organic linker unit. The IRMOF series contains ZrO_4 centers, which link with different carboxylate groups. The increase of the linker length brings about an increase in pore size and pore volume, as shown in N_2 adsorption in IRMOF-1, -10, and -16 [37].

The pore size and shape and properties of pore wall also affects the type of adsorption isotherms; Type I to Type VI (see Fig.8). For example, microporous systems give Type I isotherm and weak fluid-solid interacting systems exhibit Type V isotherm. Thus various properties and structures of PCPs' frameworks, compared with other microporous materials~~,~~ such as zeolites and activ~~e~~ated carbons may bring about unexpected isotherms.

5. Changing the ligand functionalization

Functionalizing the organic linkers with various chemical groups is an effective method to modify ~~tune~~ the physico-chemical properties of the PCPs frameworks with the aim to arrange their adsorptivity and selectivities. For example, polar – NH_2 groups were introduced on the organic ligands while keeping their original topologies with the purpose to create more efficient CO_2 uptake PCPs [37].

The ligand functionalization equally affects the selectivity, which can be significantly enhanced in the low pressure region, as was experimental observed and predicted for various PCPs such as some MILs and the ZIF, IRMOF and DMOF series. With increasing pressure, the impact of the functionalization becomes much less pronounced as the major part of the amino groups is not available anymore. Some PCPs have proven to show even higher selectivity with more polar function such as $–SO_3H$ and $–CO_2H$ groups paving the way to tune materials as highly selective as the most commonly used zeolite 13X in industrial applications [37].

In flexible PCPs, the functionalization induces the modification of not only their physico-chemical properties, but also~~,~~ the pore opening that can modify their adsorption properties. Typically, while the functional group has generally only a minor effect on the storage capacity of rigid PCPs, a significant enhancement in both properties is obtained for a polar n-alkane in the halogenated (-Br, -Cl) functionalized MIL-53(Fe) solids due to their higher degree of initial pore opening compared to the parent structure, which is

controlled by the steric hindrance of the functional group. In the case of MIL-53(Al) solid, the $-NH_2$ functional group affected positively its selective adsorption of CO_2, but this is not related to the expected additional CO_2/-NH_2 interactions but rather to its indirect impact on the flexibility of the framework.

This is, for instance the case of the MIL-53 (Fe), where the CO_2/framework interactions are not strong enough to overcome the intra-framework hydrogen bonds involving-NH_2, which leads to no CO_2 adsorption uptake in this material [37].

1.3.5. Application of multifunctional PCPs

There are a few difficulties that encounter in using PCPs, which can suffer from the following shortcomings: limited resistance to thermal degradation, instability of moisture, high cost of synthesis, and low apparent density arising from, porous structure. This low density is to be taken into account in most industrial applications where the volume occupied by the adsorbent is limited, for example, in gas storage containers and gas separation units. On the other hands, PCPs can provide high values of these specific properties or adsorptivity (per unit mass), since PCPs may have ordinary values of adsoptivity (per unit volume). For this reason, a fair comparison of PCPs with other adsorbents should often be made on a volumic basis.

There are many PCPs, which are thermally robust, water resistant, chemically resistant, and not too expensive to prepare. Thus, many potential applications of these PCPs suggested: gas storage, molecular separations [38], drug delivery [39], catalyst [40], luminescence [41], chemical sensing [42], and ionic/electronic conductivity [43].

1.4. Magnetic orientation of crystals

A molecule usually has magnetic anisotropy. Therefore, the magnetic energy of molecular systems is orientation-dependent and molecules undergoes the most stable molecular orientation. However, the energy of the molecule is negligibly small compared with the thermal energy at room temperature, and as a result, the magnetic orientation of a single molecule is expected to occur only at very low temperatures [44].

In contrast to the magnetic energy of a molecule, aggregates, having an order structure like a crystal, can obtain anisotropic magnetic energies larger than the thermal

energy at room temperature. This is because the anisotropic magnetic energy of an aggregate increases with increasing volume, whereas its translational thermal energy, is constant, regardless of volume. For the purpose of simplicity, it's assumed here that an aggregate is composed of n moles of molecules, has a cylinder shape and has molecular diamagnetic susceptibilities $\chi_{mol\perp}$ and $\chi_{mol\,II}$, which are the susceptibility perpendicular and parallel to the cylindrical axis, Z as shown in this below Figure 7. Then the magnetic energy E_{mag} of the aggregate in a magnetic field, H, is given by the following equation;

$$\begin{aligned} E_{mag}(\theta, H) &= -(1/2)\,\mu_0 n\,(\chi_{mol\,II}\cos^2\theta + \chi_{mol\perp}\sin^2\theta)\,H^2 \\ &= -(1/2)\,\mu_0 n\,(\chi_{mol\perp} + (\chi_{mol\,II} - \chi_{mol\perp})\cos^2\theta)\,H^2 \\ &= -(1/2)\,\mu_0 n\,(\chi_{mol\perp} + \Delta\chi_{mol}\cos^2\theta)\,H^2 \qquad (3) \end{aligned}$$

where θ is the angle between the magnetic field and the cylindrical axis, Z, and $\Delta\chi_{mol}$ ($=\chi_{mol\,II} - \chi_{mol\perp}$) is the anisotropic magnetic susceptibility.

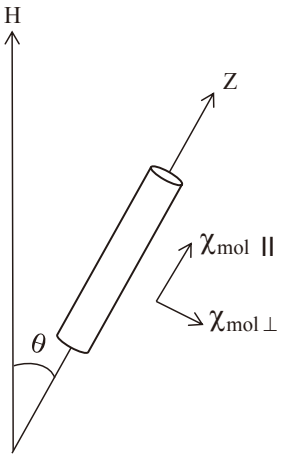

Figure 7. A cylindrical aggregate in a magnetic field. H, magnetic field; Z, a cylinder-axis of aggregate; θ, angel between Z and H. $\chi_{mol\,II}$, molar magnetic susceptibility of an aggregate parallel to Z; $\chi_{mol\perp}$, molar magnetic susceptibility of an aggregate perpendicular to Z; [44].

For molecules having lower symmetry than cubic symmetry, the magnetic susceptibility is anisotropic, i.e., (dependent on direction), and thus the magnetic energy is anisotropic. The anisotropic magnetic energy ($\Delta\chi nH^2/2 = 8.3 \times 10^{-26}$ J) for one

molecule with magnetic susceptibility ($\Delta\chi$ = 100 x 10^{-6} cm^3 mol^{-1}) in a strong magnetic field (H = 100 kOe) is much less than the thermal energy ($kT/2$ = 2.1 x 10^{-21} J, k: Boltzmann constant) at T = 300 K. When crystals are formed with an ordered structure by the arrangement of anisotropic molecules, the magnetic energy anisotropy becomes as large as the thermal energy, and the crystals are oriented in the magnetically stable direction by the magnetic torque against the thermal disordering [44].

1.5. Adsorption Isotherms

Adsorption is the accumulation of atoms or molecules on the surface of a material. This process creates a film of the adsorbate (the molecules or atoms being accumulated) on the adsorbent's surface. Desorption is the reverse process. Adsorption is different from absorption, in which a substance diffuses into a liquid or solid to form a solution. Adsorption is usually described by isotherms, that is, the amount of adsorbate on the adsorbent as a function of its pressure (if gas) or concentration (if liquid) at constant temperature. The quantity adsorbed is normalized by the mass of the adsorbent to allow comparison of different materials [3].

Adsorption is a consequence of surface energy, similar to surface tension. Atoms on the surface experience a bond deficiency because they are not wholly surrounded by other atoms. Thus, it is energetically favorable for them to bond with surface atoms. The exact nature of the bonding depends on the produced species. The adsorbed material is generally classified by physisorption and chemisorption.

1. Physisorption is a type of adsorption in which the adsorbate interacts weakly with the surface only through Van der Waals forces.
2. Chemisorption is a type of adsorption where a molecule interacts with a surface through\the formation of a chemical bond [3].

Guest molecules physisorbed onto the solid surface play an essential role in determining the properties of porous compounds (Table 1). The adsorption is governed not only by the interaction between guest molecules and the surfaces but also by the pore structure (pore size and shape). The adsorption by a macropore and single surface, are understood by the Brunauer–Emmett–Teller (BET) equation. The adsorption by a mesopore is dominated by capillary condensation, which is responsible for a sharp

adsorption rise around the mid relative-pressure region and illustrated well by the Kelvin equation, based on capillary condensation of adsorbates. The adsorption in the micropore should be considered as the filling of molecules into a nanopore where a deep potential field is generated by the overlapping of all the wall potentials. The adsorption isotherm for the microporous materials shows a steep rise at very low relative pressure and a plateau after saturation. On the other hands, the adsorption isotherm for chemisorptions was given as the Langmuir isotherm, which forms a monolayer film on solids.

There are six representative adsorption isotherms as shown in Figure 7, that reflect the relationship between pore structure and sorption type. These adsorption isotherms reveal characteristics of adsorbents that are microporous (Type I), nonporous and macroporous (Types II, III, and VI), and mesoporous (Types IV and V). When the fluid–solid attractive interaction is stronger than that of fluid–fluid, the adsorption isotherm should be of Types II and IV, and opposite situation leads to Types III and V. The Type VI isotherm represents adsorption on nonporous or macroporous solid surfaces where stepwise multiplayer adsorption occurs [3].

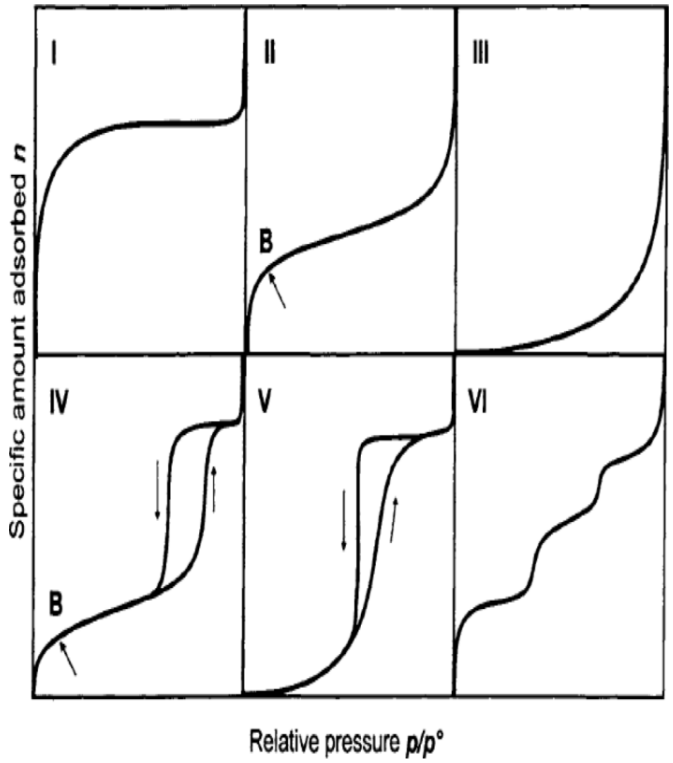

Figure 8. IUPAC classification of adsorption isotherms [3].

1.6. Adsorption isotherms of porous coordination polymers.

PCPs represent a new class of crystalline porous material with advantages such as easiness in design and synthesis, high porosity, and tunable pore properties. Because of their porosity, the most prominent property of PCPs investigated is undoubtedly their gas adsorption behavior. PCPs hold several records between porous material such as the highest surface area, the highest hydrogen uptake based on physical adsorption, and the highest storage of methane, and CO_2. Therefore, PCPs are promising candidates for CO_2 separation. The adsorptivity for CO_2 in new adsorbents may be evaluated by many factors, such as adsorption capacity, selectivity, adsorption rate, etc. However, usually CO_2 adsorption capacity is paid much more than the adsorption dynamics. Thus, the adsorption equilibrium is first measured either gravimetrically or volumetrically [45].

Most of PCPs adsorption isotherms are a Langmuir type, where at low CO_2 partial pressure adsorption amount increases steeply and linearly with pressure. Few PCPs exhibit other types of isotherms such as stepwise, sigmoidal, and hysteretic isotherms. In contrast, flexible PCPs usually result in stepwise adsorption for CO_2 and other gasses. The flexibility of CPCs is a unique property, which shows great potential in selective adsorption or separation of small molecules [45].

PCPs more than one hundred have been reported for CO_2 adsorption. Adsorption isotherms at low temperature and normal pressure are, useful in evaluating the adsorption properties, testing the CO_2 selectivity, and optimizing the design of PCPs. Furthermore, the adsorption under high pressure is directed to the evaluation of the total CO_2 storage ability of PCPs. CO_2 storage capacity in PCPs can be enhanced in various ways, as exemplified below:

1. Increasing surface area.

Generally speaking, adsorption amount will be proportional to the surface area of adsorbents, irrespective of adsorbates. Amount of CO_2 adsorbed also increased with increasing specific surface area. Therefore, one of strategies is increase in the surface area of PCPs. CO_2 adsorptivity of various PCPs was explored and found that it was enhanced by increase in their surface areas, as shown in Figure 10 [45].

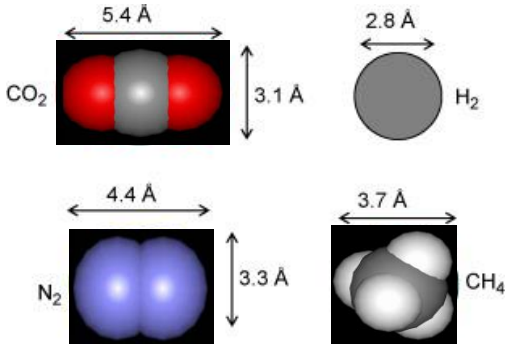

Figure 9. The approximate molecular dimensions of CO_2, H_2,N_2 and CH_4 [45].

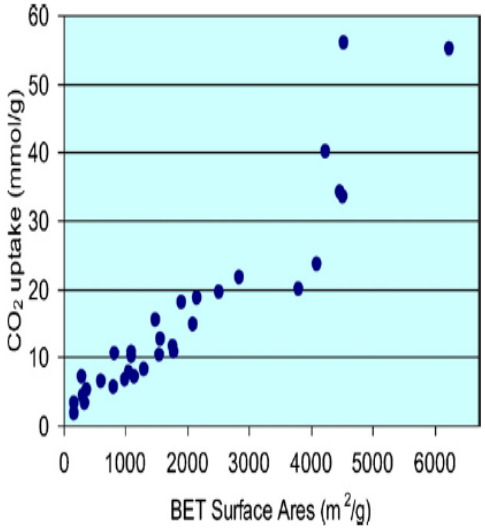

Figure 10. Experimental ~~of~~ CO_2 uptake in different PCPs [45].

2. Functionalizing organic linker~~-~~

The organic linkers with diverse chemical groups were used to tune the physico-chemical properties of the PCP frameworks (polarity, acidity, basidity, etc), which may lead to modulate their adsorption capacities and selectivities. The functionalization of linkers is achieved by either using simply linkers containing the desired functional group or post-synthetic modification. One of the active endeavors on PCPs is to graft polar NH_2 groups on the organic ligands to adsorb more efficiently CO_2, while keeping their original topologies. The ligand functionalization equally affects the selectivity which can be significantly enhanced in the low pressure region.

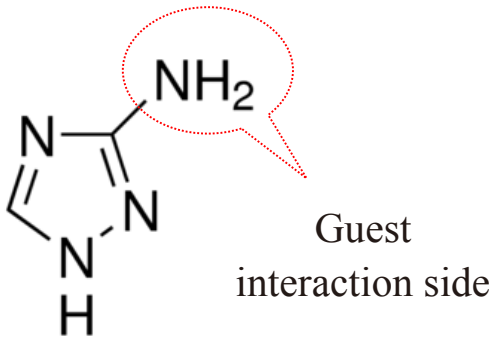

Figure 11. One of example ligand for PCPs synthesis with amine functionalized.

1.7. PCPs comprising triazole frameworks

Many PCPs are built from the aromatic carboxylate using as ~~based~~ secondary building units from the view point of certain positive aspects. Combinations with N-heterocyclic compounds (imidazole, pyrazole, triazole, tetrazole, etc) were also conducted because of their various binding and bridging modes. 1,2,4-triazole and its derivatives, have gained more and more interest as ligands, because they are usually studied as the precursors of compounds important in medical biology and industry. These ligands connect the coordination of both pyrazole and imidazole and exhibit an extensively documented ability to bridge metal ions and afford polynuclear clusters. Many triazole-based polynuclear compounds have been reported, including dinuclear, linear trinuclear, cyclic trinuclear, tetranuclear, and hexanuclear ring complexes.

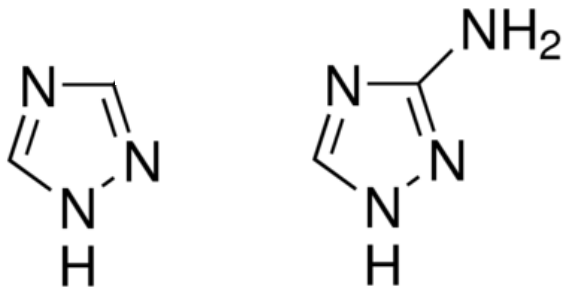

1,2,4-triazole 3-amino,-1,2,4-triazole

Figure 12. Structures of 1,2,4-triazole and 3-amino,-1,2,4-triazole

An amine group connected to 1,2,4-triazole gives different properties of 3-amino-1,2,4-triazole for guest molecules interaction especially CO_2 molecules. Some investigations on CO_2 adsorptivity of amine-containing appeared in the recent literature.

1.8. Outline of This Research

The overall aim of this research is to synthesize a new PCPs comprising triazole and oxalate ligands. This approach contains CO_2 adsorption for produce notable pore volume and the use of high magnetic fields for modification of pore structures.

Each chapter is a self-contained unit that summarizes the results of various PCP systems that were explored in the study. The introduction at the beginning of each chapter will highlight the focus of the section at hand. Chapter 2 explores new design of PCPs as $Zn_2(C_2O_4)(C_2N_3H_2)_2.(H_2O)_{2.5}$ or $[Zn_2(Oxac)(Taz)_2]\cdot(H_2O)_{2.5}$ ($ZOTW_{2.5}$) with triazole ligands with no mine groups presence which may promoted pore volume to accept carbon dioxide molecules. This new PCP exhibits a new micropore formation route via water-assisted CO_2 adsorption.

In Chapter 3, we report PCPs prepared from the same reactant solutions as $ZOTW_{2.5}$ under magnetic fields of up to 6T. Magnetic fields effects on pore structures of the PCPs, such as pore volume and properties, are reported.

Chapter 2 Micropore formation of $[Zn_2(Oxac)(Taz)_2]\cdot(H_2O)_{2.5}$ via CO_2 adsorption

2.1. Introduction

Porous materials are widely used for adsorbents such as separation, catalytic supports, electric capacitor substrates, and so forth. The adsorptivity of adsorbents depends on physical properties such as pore size and shape, hydrophobicity and charge density of pore wall, along with chemical properties such as surface functional groups. Porous coordination polymers (PCPs) [46-49] and metal organic frameworks (MOFs) [50-53] are constructed from metal ions and organic linker ligands to give two- and three-dimensional frameworks. PCPs are attractive porous materials, because they are crystals which lead to homogeneous definite pores and their structures and functions are easily controlled by changing organic ligands and metal ions. Various designed PCPs were prepared from physical and chemical points of view [52]. For example, gas storage capacity in PCPs was promoted by introducing open metal sites [53], increasing surface area,[54] and modifying pores using functionalized organic linker [51,55,56]. Using a ligand containing an amino group such as aminotriazole (ATaz), no micropores appeared, but CO_2 can be adsorbed because of interaction between amino groups and CO_2 [51].

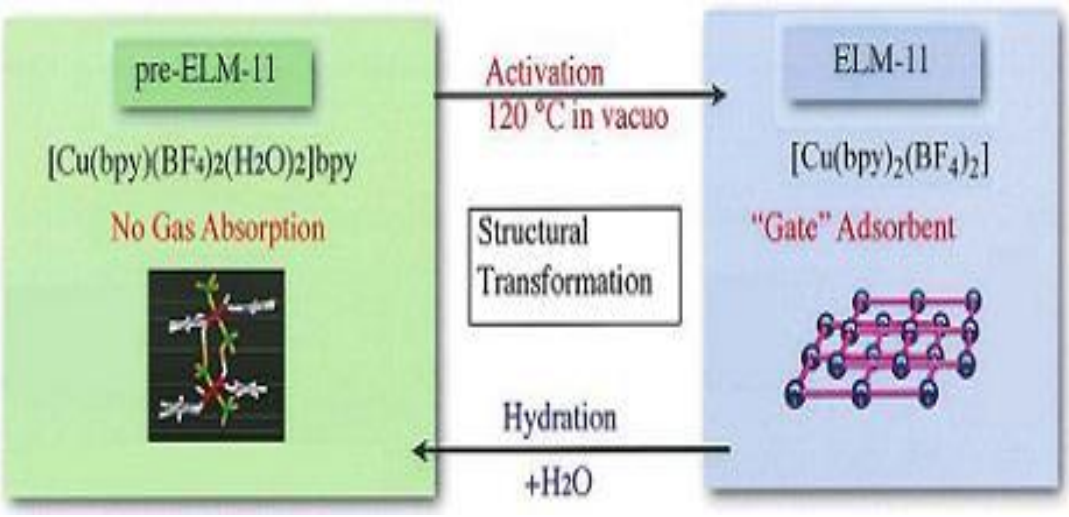

Figure 13. Structure transformation between pre-ELM-11 and ELM-11 [50].

A unique adsorption mechanism, the gate phenomenon, [47,57] was found that the latent pores of PCPs were opened above a critical pressure [57]. A flexible PCP, e.g., ELM-11, adsorbed CO_2 in the gate mechanism, which was brought about after dehydration due to heating the pre-ELM-11 having no gas adsorptivity. Such gate adsorption was observed in CO_2 adsorption on $\{Zn_2(C_2O_4)(C_2N_4H_3)_2\}(H_2O)_{0.5}$ [71], referred to $ZOATW_{0.5}$. Amount of solvent and functional groups inside frameworks of PCPs is very important for formation of latent pores and their flexibility as well as pore volume and adsorptivity.

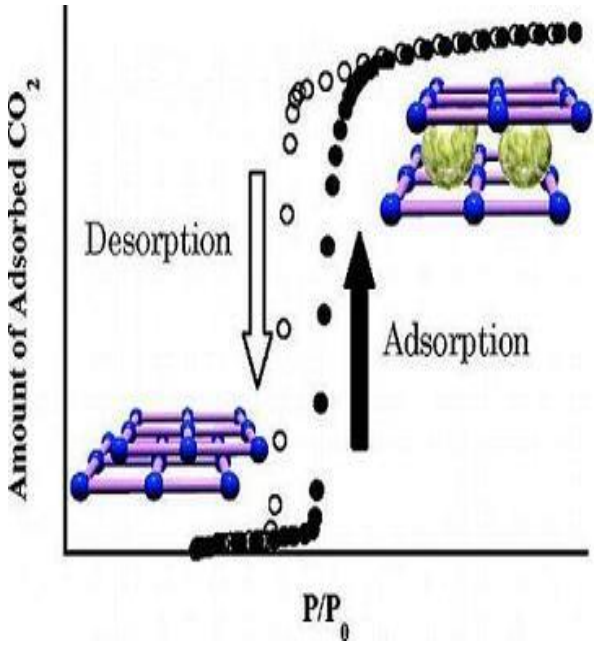

Figure 14. Schematic representation of the gate adsorption of CO_2 of ELM-11[54].

Mostly, flexible frameworks are characterized by stepwise adsorption and presences of solvent inside the pore could induced a new interesting pore properties on PCPs with structural flexibility. The effects of benzene as solvent which is arranged in the cage of PCPs is accommodated strongly in the cavity with the size effect and interaction with the framework of Zn(μ4-TCNQ-TCNQ)bpy].1.5benzene. Presence of benzene in frameworks could be removed at 413K for 10 hours under low pressure and then this frameworks can capture gas molecule. This framework also formed as flexible /

dynamics frameworks due to their gate phenomena observed in oxygen (O_2) adsorption isotherms [47].

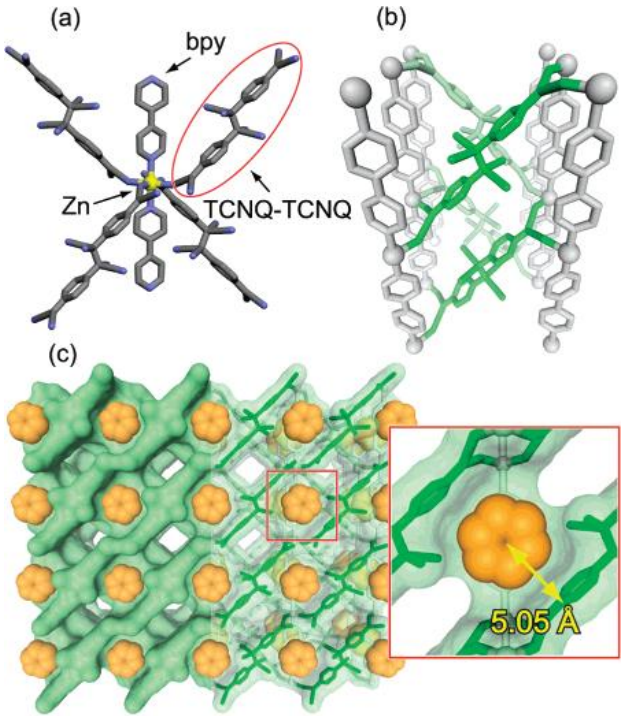

Figure 15. (a) Coordination environment of Zn(II) ion of **1**_benzene. (b) TCNQ dimer (green) connected to four 1D chains of Zn and bpy (gray). (c) Benzene arranged in the cage of the undulating channel of **1**_benzene [47].

In this study, we report a new route for micropore formation of PCPs via CO_2 adsorption in micropores containing water. An as-synthesized crystal of $[Zn_2(Oxac)(Taz)_2]\cdot(H_2O)_{2.5}$, $ZOTW_{2.5}$ having no pores, was prepared by solvothermal reaction of Zn^{2+}, 1,2,4-triazole (Taz) and oxalic acid (oxalate ion is abbreviated to Oxac). Although the as-synthesized $ZOTW_{2.5}$ pretreated gently had little open micropores and thus adsorbed only small amount of CO_2, the CO_2-adsorbed PCP brought about large micropore volume after being degassed at around room temperature. 1,2,4-triazole was selected as main ligand because this compound have developed as flexible characteristic and dynamic structural transformation. Oxalic acid with 2 carboxylate groups can act as linker ligand to build 3 dimensional structure of PCPs.

2.2. Experimental Section

0.4g of $Zn_5(CO_3)_2(OH)_6$ (Alfa Aesar, Co. Ltd.), 0.4g of Oxac (Wako Pure Chemical Industries,Ltd.; WPCI), and 1.4g of Taz (WPCI) were added to a mixed solvent of 12mL of methanol (WPCI) and 2mL of distilled water. The solution containing white precipitates was transferred to a Teflon cell which was set in an autoclave vessel, and heated at 453 K for 12 h. Cooling the system to room temperature, the prepared crystals (Fig. 16) were filtered with a membrane filter and washed with the solvent, followed by drying in air at room temperature. In order to obtain pure crystals, the molar ratio of reactants was varied in narrow range.

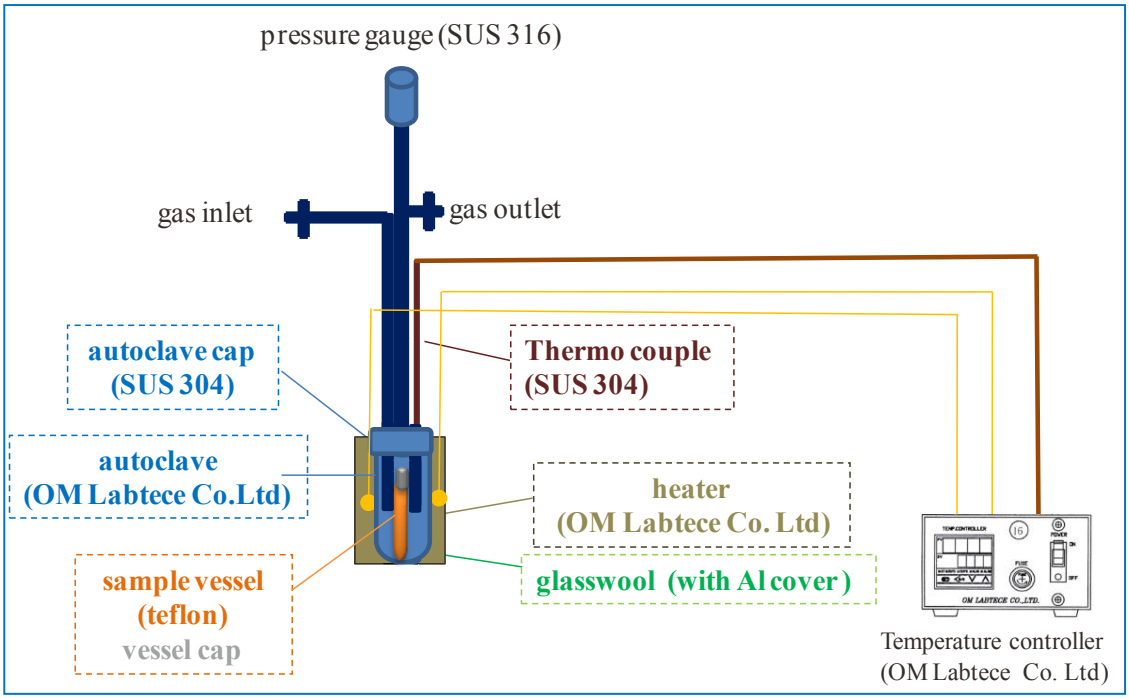

Figure 16. Synthesis method and design of $[Zn_2(Oxac)(Taz)_2]\cdot(H_2O)_{2.5}$, $ZOTW_{2.5}$

The prepared crystals were characterized by a Rigaku X-ray diffractometer (XRD) Multiflex with Cu Kα at 40 kV and 20 mA and a JEOL scanning electron microscope (SEM) JSM-7600F. The crystal structure was initially estimated by the program EXPO2014 [19], and successively refined by the Rietveld method using RIETAN-FP program [58]. Thermogravimetric and differential thermal analysis (TG/DTA) were carried out using a Rigaku Thermo Plus TG8120. Also, amount of solvent included in ZOTs was examined gravimetrically as a function of heating time at 383 K. The

elementary analysis of C, H, and N was carried out with a Thermo Electron Flash EA1112 elementary analysis equipment.

N_2 and CO_2 adsorption was measured at 77 and 303 K, respectively, using a custom-made volumetric adsorption system as shown in Fig. 17. Each sample of ca. 100 mg was pretreated at 383 K and 1 mPa for various times, t_{pt}/h. To confirm the N_2 adsorption amounts a gravimetric method was also carried out with a quartz spring (the spring constant of 5.829 mg/mm). Carrying out a series of adsorption experiments, an as-synthesized PCP was pretreated only before first adsorption, and subsequent adsorption experiments were done after degassing at 1 mPa and 298 K for 30 min.

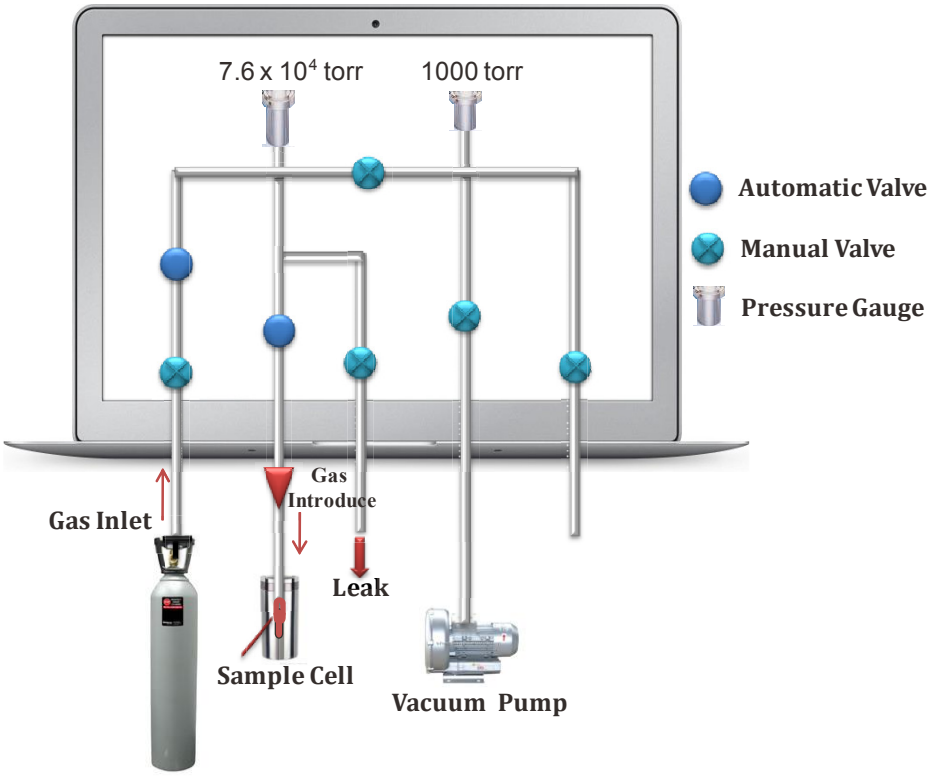

Figure 17. Volumetric adsorption isotherms apparatus

The infrared (IR) spectra were measured by a JASCO VIR-200 infrared spectrometer, using a vacuum cell with CaF_2 windows connected to a vacuum line. The sample powder of 2 mg was filled in 0.5 mm-thickness, evacuated for 5 min, followed by CO_2 gas introduction, and then its IR spectra were measured with a transmission method.

2.3. Results and Discussion

White crystals of Zn-Oxac-Taz complexes (ZOT) were synthesized in the yield of ca. 70 %. The composition was estimated $[Zn_2(C_2O_4)(C_2N_3H_2)_2]\cdot(H_2O)_{2.5}$, which is referred to as $ZOTW_{2.5}$, from the results of TG and elementary analyses (C : H : N = 18.02 : 2.27 : 21.02 %).

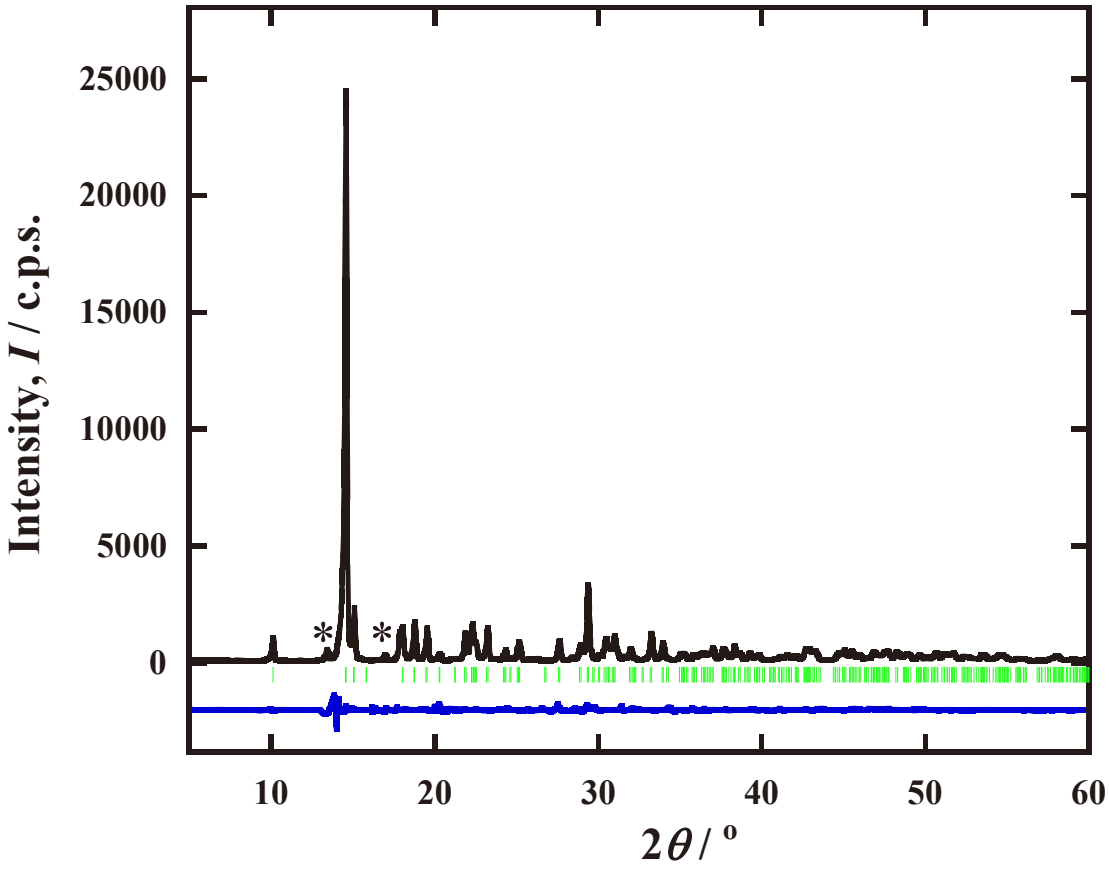

Fig. 18. The experimental XRD pattern (top) of an as-synthesized $ZOTW_{2.5}$, $[Zn_2(C_2O_4)(C_2N_3H_2)_2]\cdot(H_2O)_{2.5}$. *: Impurity peaks. Peak positions simulated by the Rietveld method are shown (middle). The residue (bottom) between the experimental and simulated peak intensities are plotted

The XRD pattern of a pure crystal (Fig. 18) was selected from various prepared crystals by the plots of XRD intensities of all peaks as a function of composition of

reactants in preparing. The XRD peaks could be indexed in the monoclinic system, P_{21}/a. Fig. 18 includes the results of the Rietveld refinement using the XRD pattern ($2\theta/^{o}$ = 5 ~100) without tiny impurity peaks around 13° and 17°, whose fit was fair as the residual intensity shows (table 2, in pp. 48-50).

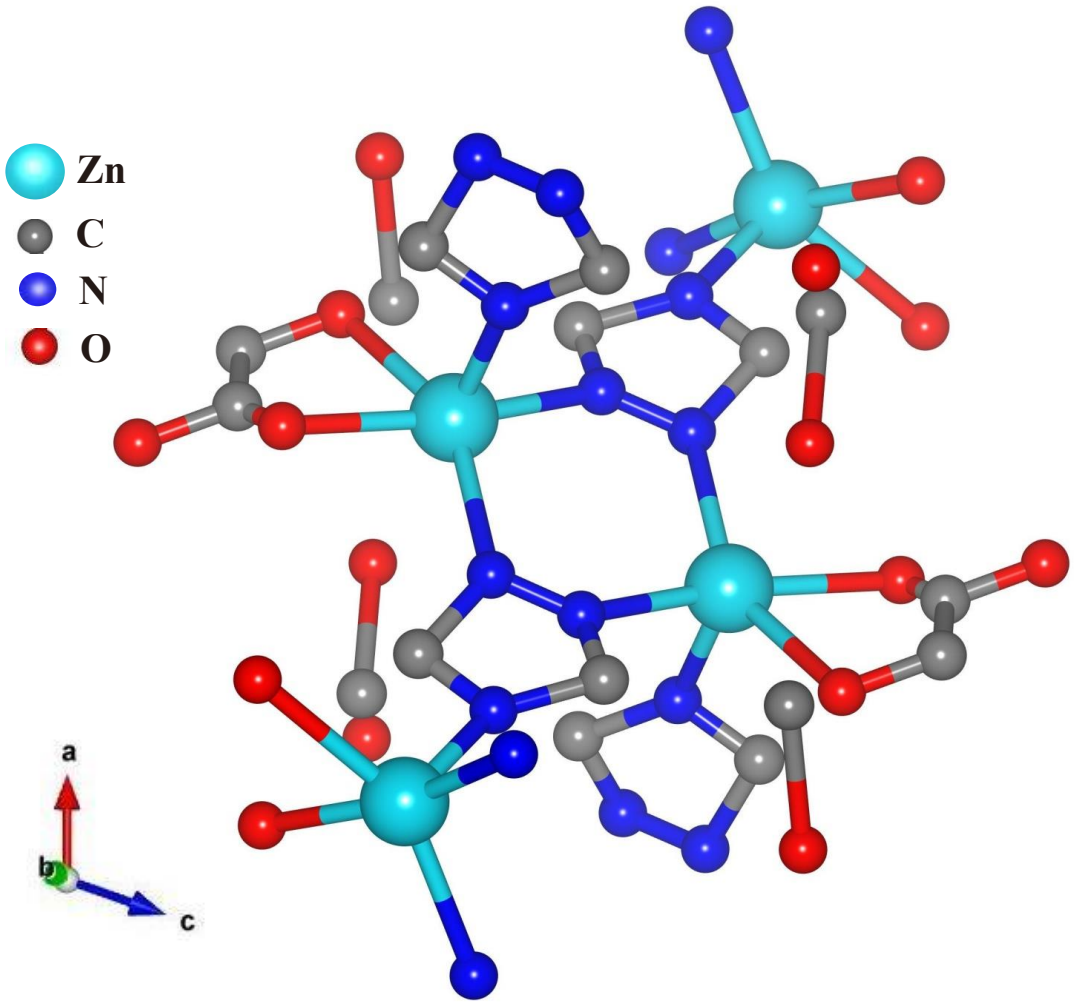

Figure 19. Local crystal structure of $Zn_2(C_2O_4)(C_2N_3H_2)_2 \cdot (H_2O)_{2.5}$
Color scheme: Zn-cyan, N-blue, O-red, C-gray

Fig. 19 and 20, constructed by Vesta program [74], depict the crystal structure (without H_2O) of the as-synthesized $ZOTW_{2.5}$, having a five coordinated Zn^{2+} ion connecting to three Taz molecules and an Oxac molecule. The crystal has 3-dimensional

coordination network and micropores along the c-axis, whose size is estimated ca. 0.30 x 0.31 x 0.40 nm^3. The composition and crystal structure were very similar to $ZOATW_{0.5}$ prepared by using ATaz instead of Taz, although our pore space may be filled with water instead of amino groups, as suggested by their compositions [51].

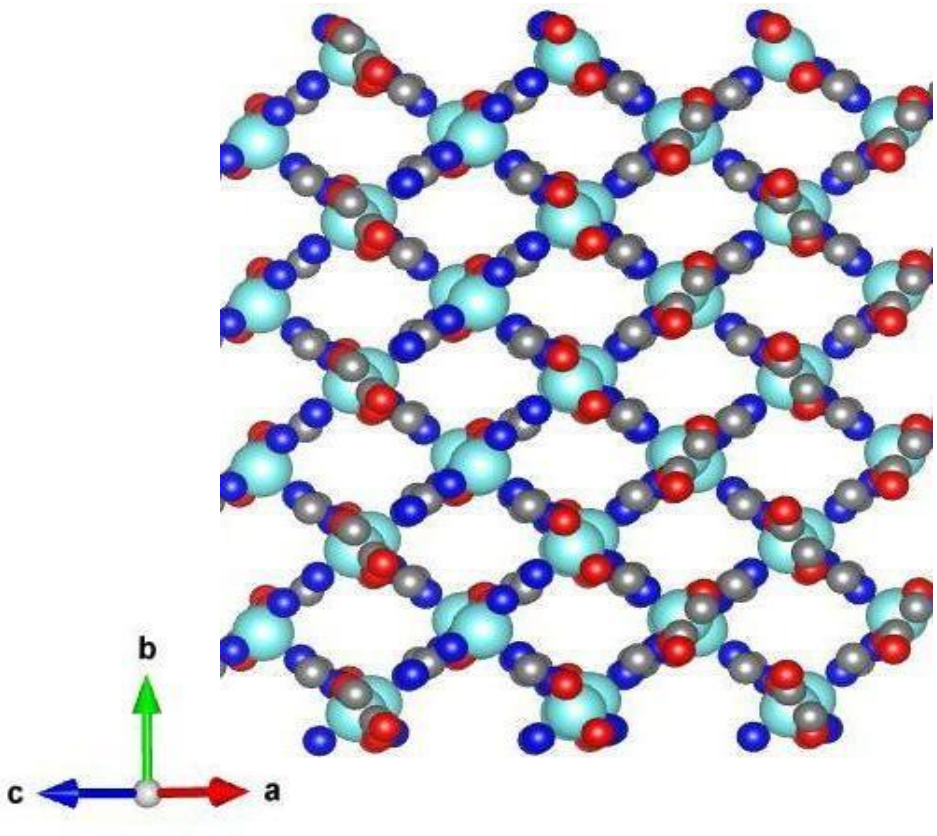

Figure 20. The crystal structure of an as-synthesized $Zn_2(C_2O_4)(C_2N_3H_2)_2 \cdot (H_2O)_{2.5}$, which was determined by the Rietveld method.

Fig. 21 shows that an as-synthesized $ZOTW_{2.5}$ has little amount of N_2 adsorbed at 77 K, indicating that the micropores are filled with solvent. As-synthesized $ZOTW_{2.5}$ for gas adsorption was pretreated at 383 K, because TG/DTA curves showed that solvent molecules included were removed between 330 and 383 K. By heating as-synthesized $ZOTW_{2.5}$ at 383 K, its weight measured using the gravimetric method decreased in sigmoid to reach a saturation value (Fig. 23). After short pretreatment the crystals still include some water to be expressed as $ZOTW_x$, where $x = 2.5–\Delta$ (Δ is the amount of H_2O

dehydrated). The pretreatment shorter than 2h brought about little change in adsorption amount of N_2, but sufficient pretreatment increased significantly adsorption amount from low pressure, whose adsorption isotherms are classified as Type I [75], indicating the appearance of micropores due to removal of H_2O. The $ZOTW_x$ pretreated over 12 h showed the saturation adsorption amount of ca. 190 mg/g (0.15 mL/g) from the DR-plot and the pore diameter of 0.7 nm from the *t*-plot [75]. Using the structural data refined by the Rietveld method, the pore volumes of $ZOTW_{2.5}$ and $ZOTW_x$(12h) were estimated with PLATON[76] to be 0.033 and 0.201 $cm^3\ g^{-1}$ (the porosity of 6.4 and 31.7 %), respectively. The values correspond to the saturation adsorption amounts of N_2, *V*s, of 26.8 and 163 mg g^{-1} and also are consistent with the experimental *V*s values. Since the size of an N_2 molecule is ca. 0.33^{Φ} x 0.44 nm^2, the frameworks seem to be somewhat flexible.

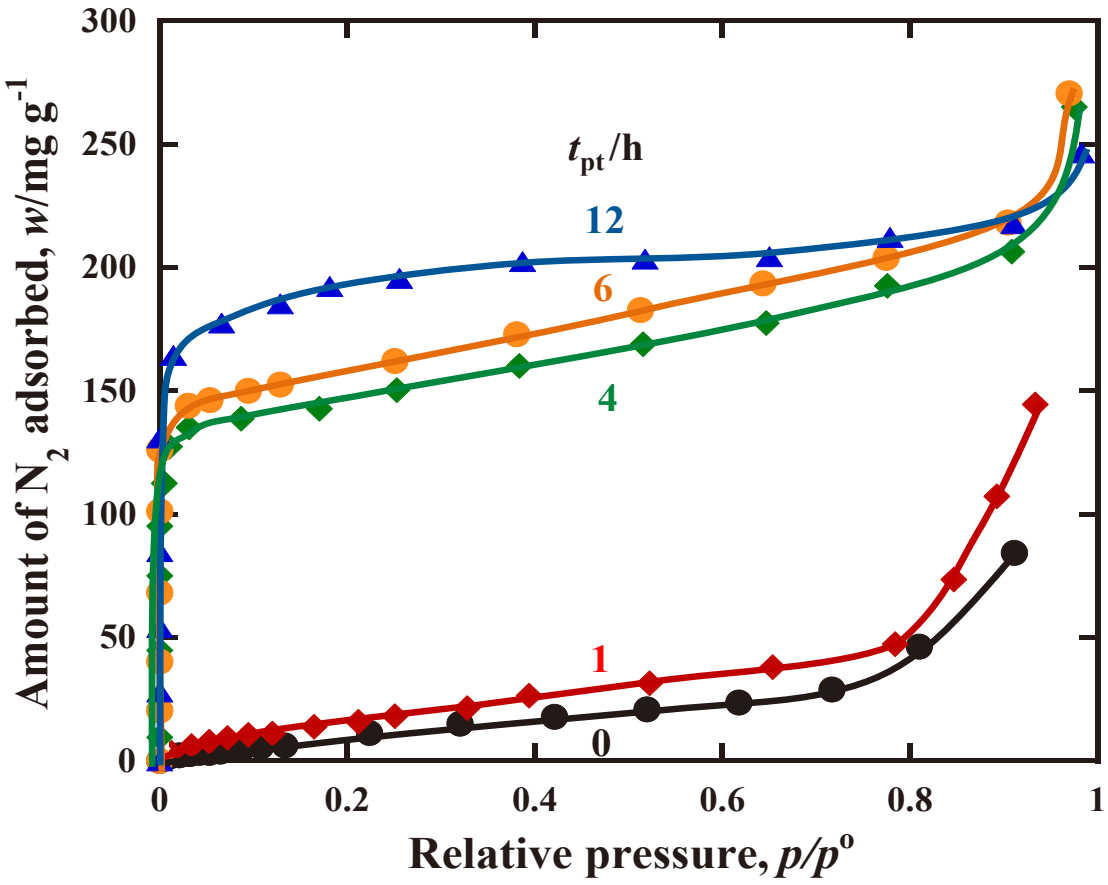

Figure 21. Adsorption isotherms of N_2 adsorbed on $ZOTW_x$ after pretreating $ZOTW_{2.5}$ for t_{pt}/h at 77K.

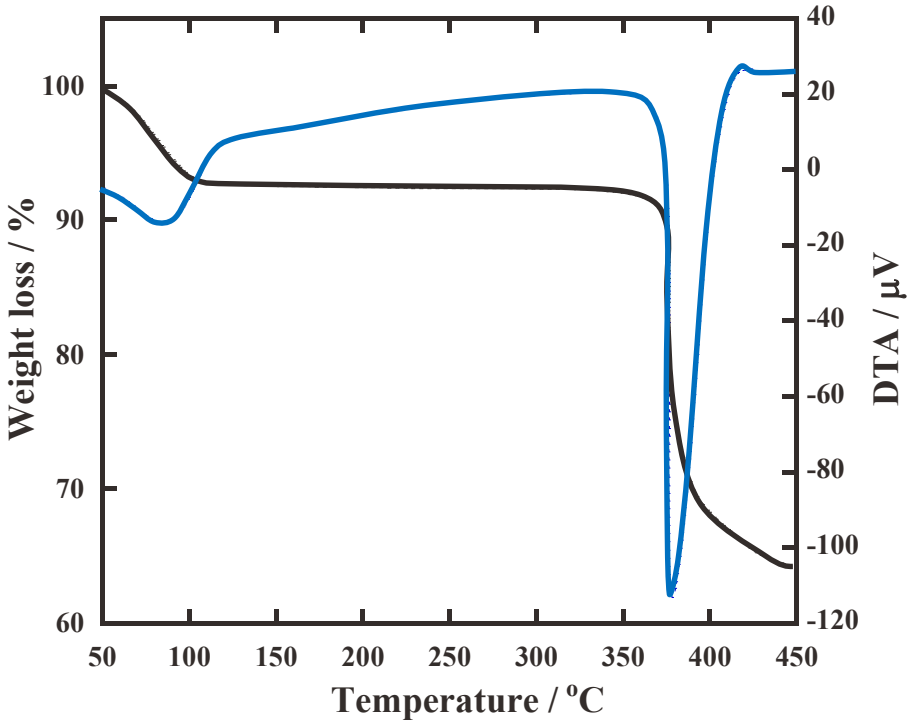

Figure 22. TG/DTA result for as-synthesized $ZOTW_{2.5}$.

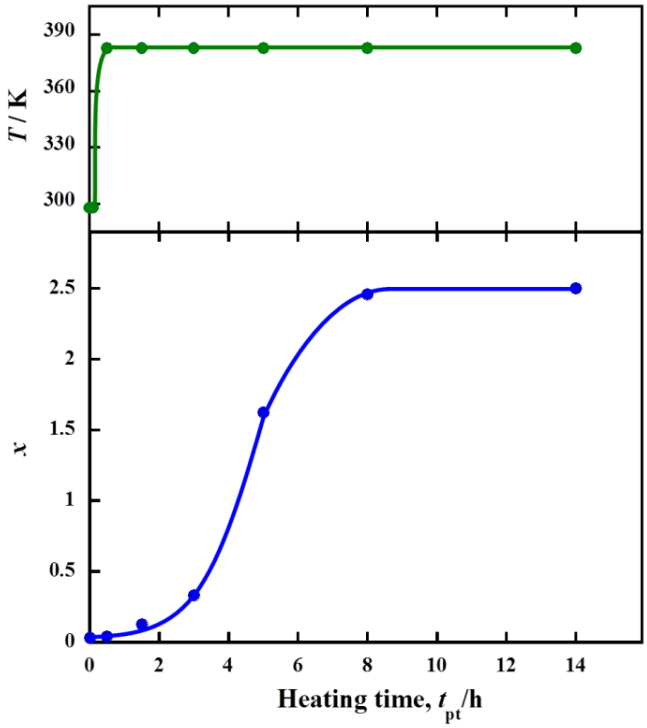

Figure 23. Change of x value of $ZOTW_x$ with heating time at 383 K and 10 mPa, which was measured by the gravimetric method.

CO_2 adsorption for $ZOTW_x$ pretreated for various t_{pt}/h was examined at 303K, as show in Fig. 24. The opened micropores of $ZOTW_x$(≥3h) pretreated over t_{pt}/h = 3 accepted CO_2 molecules from low CO_2 pressure to approach the saturation adsorption amount of up to 120 mg/g. The non-pretreated $ZOTW_{2.5}$ having no opened micropores adsorbed hardly any CO_2 molecule at low pressure, but gradually adsorbed beyond 300 Torr. With increasing the pretreatment time up to t_{pt}/h = 2, CO_2 was adsorbed in sigmoid or cooperatively in partially H_2O-filled micropores, and approached to the adsorption amount in opened micropores of $ZOTW_x$(≥3h), 120 mg/g, at high pressure region.

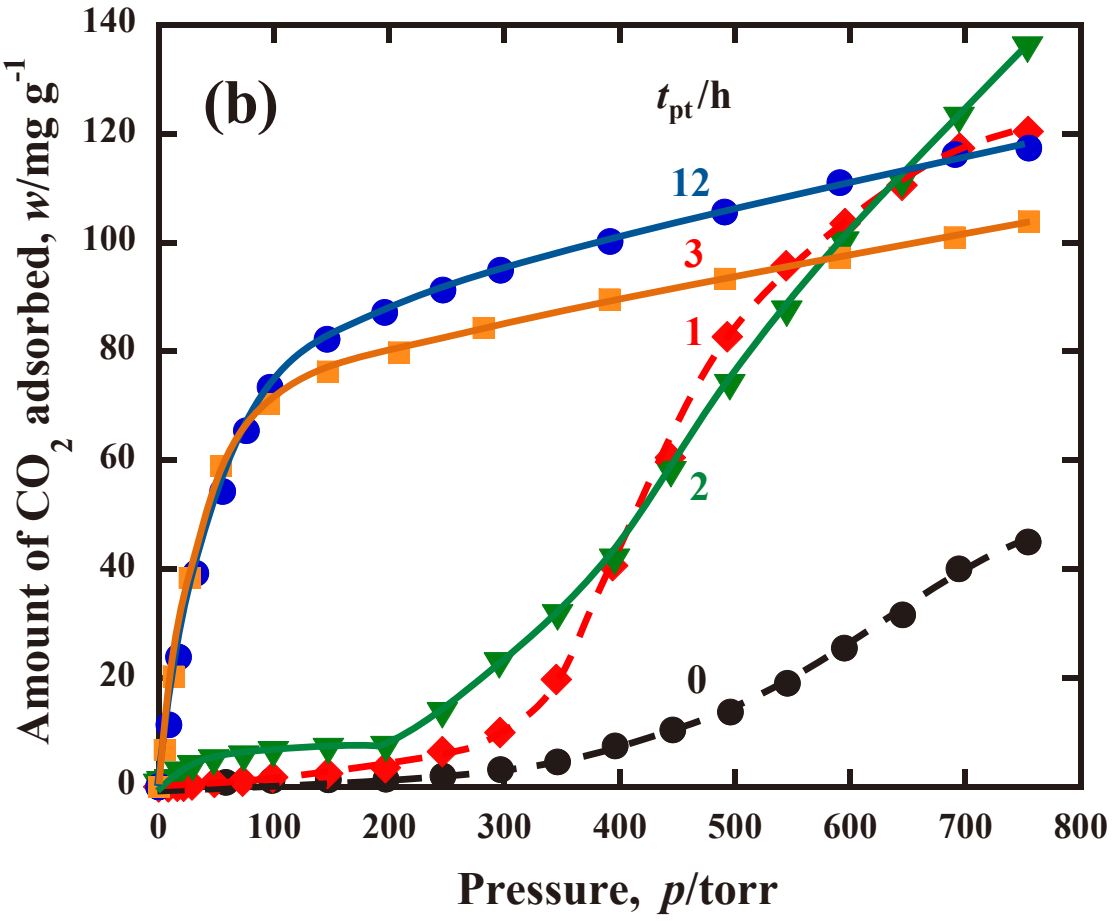

Figure 24. Adsorption isotherms of CO_2 adsorbed on $ZOTW_x$ after pretreating $ZOTW_{2.5}$ for t_{pt}/h at 303K.

The behavior may be a kind of gate opening adsorption at around 200 ~ 400 Torr of CO_2, although usually the gate phenomenon appeared stepwise [57,71]. $ZOATW_{0.5}$ showed that the open of gate for CO_2 brought about the adsorption amount of CO_2 of 1.42 times the saturation uptake of 100 mg/g. It was interpreted that the gate phenomenon arose from the presence of symmetrically positioned Zn-O bonds of the Zn-oxalate units that facilitate subtle swivelling motion [71]. Though there are little accessible micropores for N_2 in the case of t_{pt}/h less than 3h, the CO_2 adsorptivity of $ZOTW_x(\leq 2h)$ gradually increased with t_{pt} up to 7 mg/g below 200 torr and significant increase over the pressure.

The CO_2 adsorption amount expected from the solubility of CO_2 in bulk water, 14.5 mg/cm^3 at 298 K [76], is less than 0.4 mg/g. Thus, such high CO_2 adsorptivity suggests that CO_2 should interact strongly with H_2O molecules at high CO_2 pressure and be assisted by the interaction between CO_2 and pore frameworks as in opened micropores of $ZOTW_x(\geq 3h)$. A CO_2 molecule having the size of around 0.31^{Φ} nm (x 0.54 nm) seems to be more accessible than an N_2 molecule to narrow micropores at 303 K in higher fugacity region.

The high CO_2 adsorptivity seems to require the formation of a specific species occluding CO_2 in micropores comprising water and frameworks. In a preliminary IR measurement of $ZOTW_{2.5}$ under CO_2 gas, a peak of CO_2 at around 2276 cm^{-1} appeared just below the band of CO_2 gas. The peak increased with increase in CO_2 pressure of 240 to 500 Torr (0.067 MPa), and reversibly disappeared by degassing. When CO_2 was included in water as a clathrate hydrate at 3.3 MPa and r.t., the Raman bands of the Fermi diad and anti-symmetric stretching vibration of CO_2 gas shifted by 7 and 14 cm^{-1}, respectively, to lower wavenumber. [78,79] Since the anti-symmetric stretching vibration (2349 cm^{-1}) is IR-active, the 2276 cm^{-1} peak may be assigned to the vibration of CO_2 occluded in a clathrate-like species, comprising CO_2, water, and polar framework. However, the formation of such clathrate-like structure must require very high pressure.

It is reported that the effective pressure of adsorbed phase in micropores less than 1 nm in pore size is very high even under 0.1 MPa because of deep potential energy wells; [80-83] e.g., 2 GPa in micropores of CPL-1 ($[Cu_2(pzpc)_2pyz]$) [80] and 1.9 GPa [81] and 90 GPa in carbon nanotubes [81]. Thus, the 2276 cm^{-1} band suggests that certain clathrate-like species may be formed in micropores of $ZOTW_{2.5}$ because of high pseudo-pressure.

The lower shift might be brought about by extremely high pressure in micropores. Such high pressure may induce deformation of frameworks including new species and also the decomposition of the species due to CO_2-degassing may induce the removal of water as well as CO_2, followed by the formation of abundant open micropores.

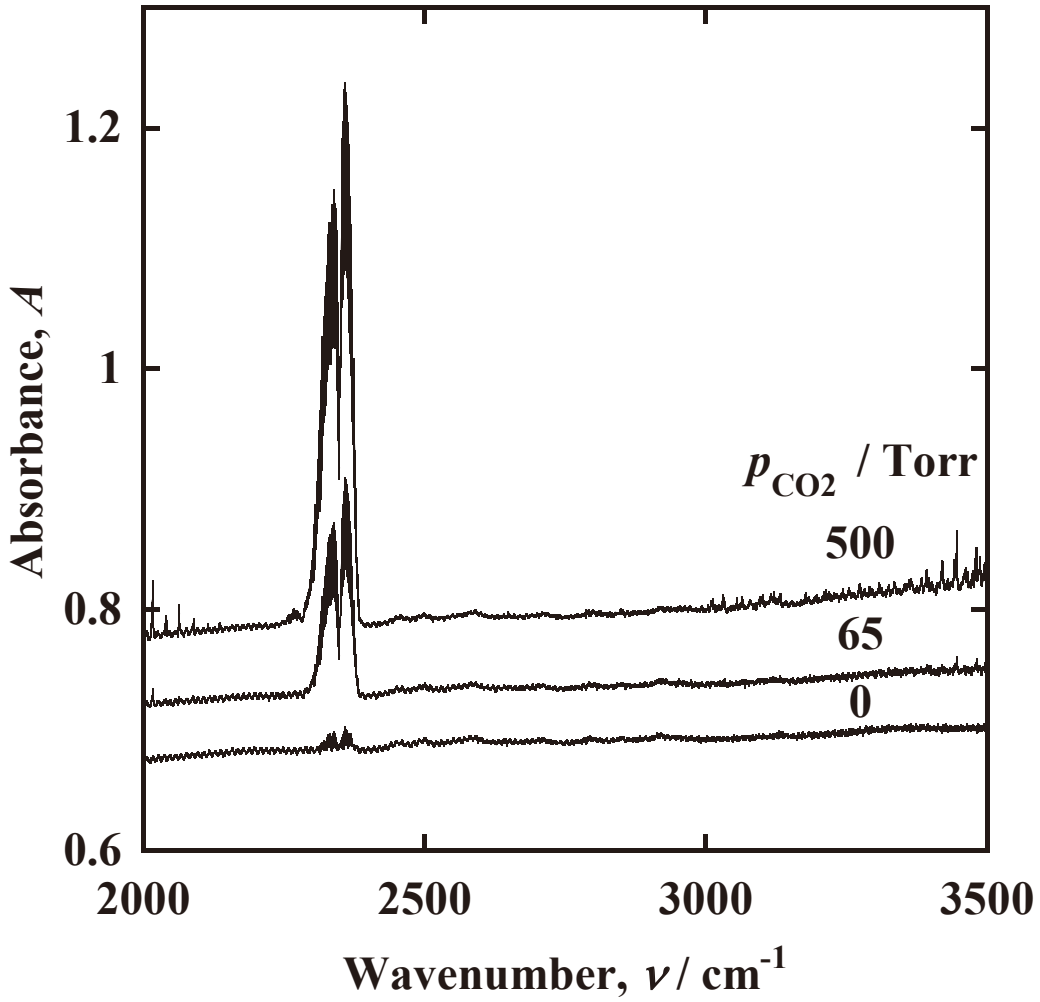

Figure 25. IR spectra of $ZOTW_{2.5}$ under CO_2 gas. CO_2 pressure, pCO_2/Torr: lower, 0; middle, 65; upper, 500. A new peak (2276 cm^{-1}) for adsorbed CO_2 species appeared under CO_2 of 500 Torr. No peak for the adsorbed CO_2 species appeared at 65 Torr, because amount of CO_2 adsorbed was much less than that at 500 Torr, as Figure 24 shows. The small peak of CO_2 gas (2349 cm-1) in the IR spectrum at pCO_2/Torr = 0 (in vacuum) arises from CO_2 gas inair along the light path in the IR equipment.

Fig. 26 shows N_2 adsorption isotherms measured at 77K for ZOTW$_x$(t_{pt}h)deCO$_2$ which was degassed at 298 K after CO_2 adsorption. The saturation amounts (w_s/mg g^{-1}) of N_2 adsorbed or micropore volumes were plotted as a function of pretreatment time (Fig. 27). Only when as-synthesized ZOTW$_{2.5}$ was shortly pretreated for t_{pt}/h≤2, amounts of N_2 adsorbed on ZOTW$_x$(≤2h)deCO$_2$ increased markedly up to 1000 mg/g, ca. 5 times larger than the w_s value of N_2 prior to CO_2 adsorption, which were much larger than values expected from the CO_2 adsorption. The size of micropores formed was almost unchanged. Such large adsorption amounts of N_2, which were confirmed by the gravimetric method, suggest that CO_2 interacting with water in micropores may induce the removal of H_2O by the gentle degassing process at 298 K to assist the formation of the micropores.

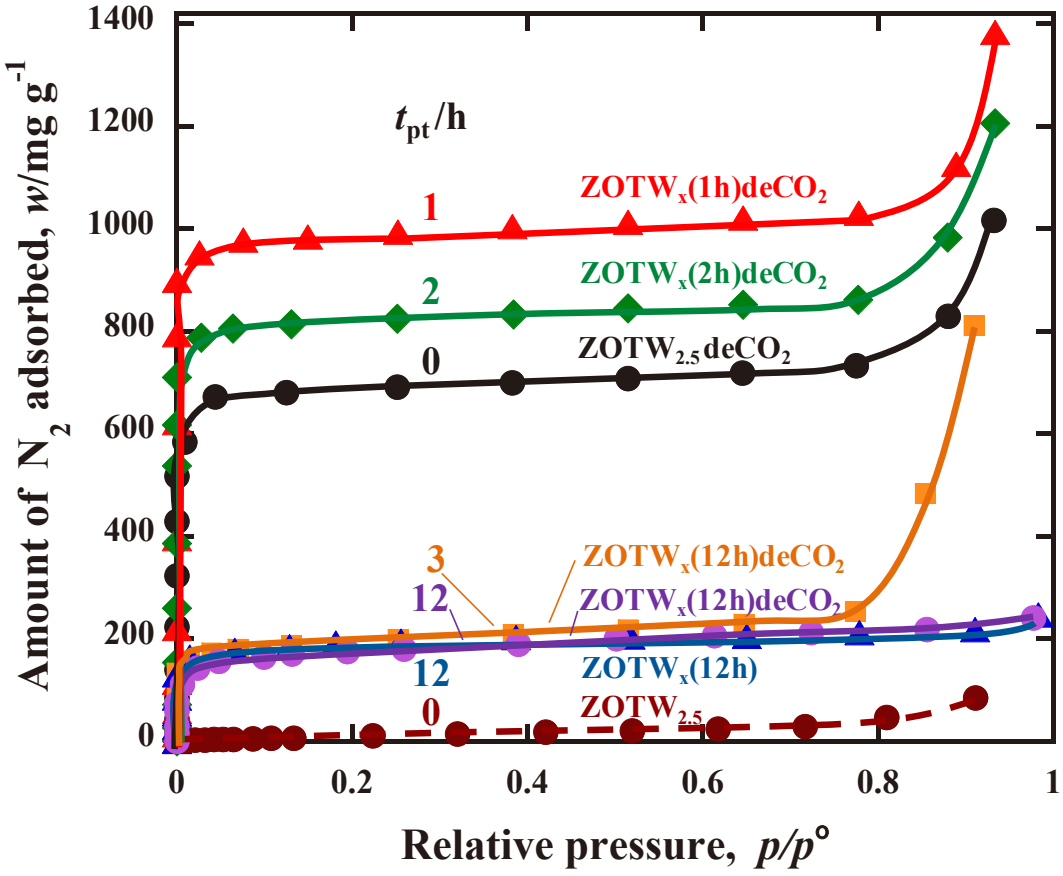

Figure 26. N_2 adsorption isotherms for ZOTW$_{2.5}$deCO$_2$ and ZOTW$_x$(t_{pt}h)deCO$_2$ (t_{pt}=1~12), measured at 77K after CO_2 adsorption shown in Fig. 24. As a reference, N_2 adsorption isotherms for ZOTW$_{2.5}$ and ZOTW$_x$(12h) are included.

Fig. 28 shows the XRD patterns of $ZOTW_{2.5}deCO_2$, $ZOTW_x(1h)deCO_2$, and $ZOTW_x(2h)deCO_2$ (not shown). They were similar to each other and slightly different from that of $ZOTW_{2.5}$. The (110) peak in the XRD pattern of $ZOTW_{2.5}$ shifted by $2\theta/^o = 0.6$ to the lower angle, which corresponds to 0.06 nm-increase in (110) spacing. On the other hand, no $ZOTW_x(\geq 3h)deCO_2$ changed their XRD patterns, suggesting that the structure should be stable. $ZOTW_x(\leq 2h)deCO_2$ samples may be a metastable structure, because the XRD pattern approached to the XRD structure of $ZOTW_x(\geq 3h)deCO_2$ after the long storage of 16 months.

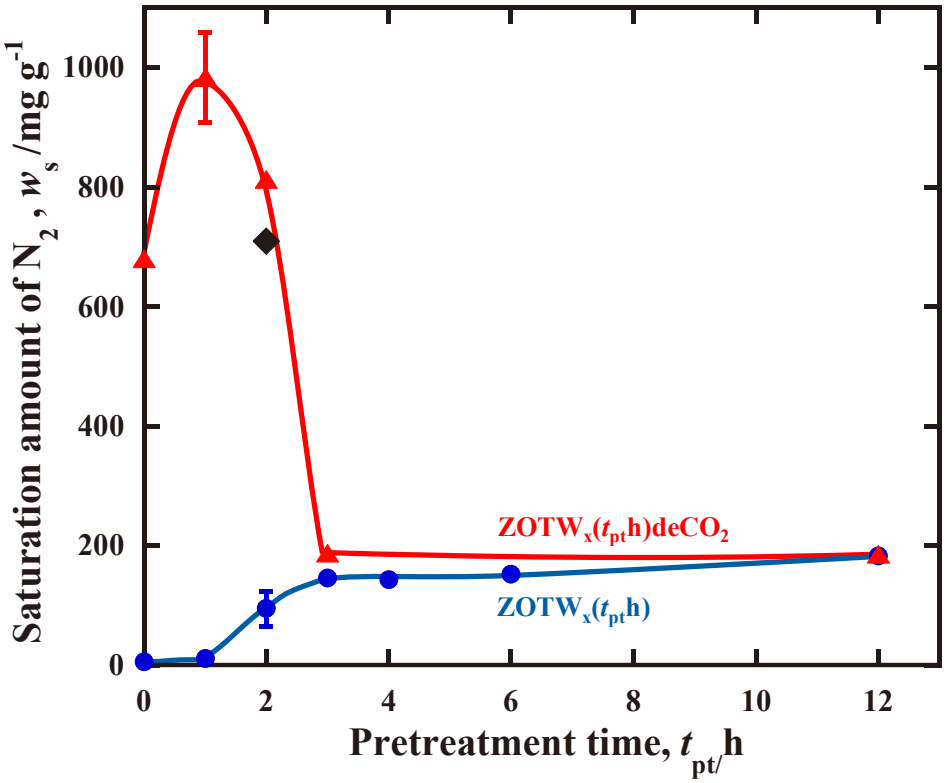

Figure 27. The saturation amounts of N_2 adsorbed on $ZOTW_x(t_{pt}h)$, blue circle, and $ZOTW_x(t_{pt}h)deCO_2$, red triangle, were plotted as a function of pretreatment time. ♦: the saturation amount of N_2 determined by the gravimetric method.

Therefore, $ZOTW_x(\leq 2h)deCO_2$ will be a mixture of slightly different structures during the structural relaxation. Thus the crystal structure, especially the structure around oxalic acid, cannot be simulated definitely by the Rietveld method. Fig. 29 A and B depict the crystal structure for $ZOTW_x(1h)deCO_2$ simulated using the molecular structure

of oxalic acid (table 3). The simulated structure is similar to that of $ZOTW_{2.5}$, but the positions and rotational angles of Taz ring and Zn-Oxac complex are slightly different. The difficulty in our structural analysis may arise from swivelling motion around Zn-O bonds of the Zn-oxalate units, as observed in $ZOATW_{0.5}$, and such rotational flexibility may bring about the remarkable increment in micropore volume.

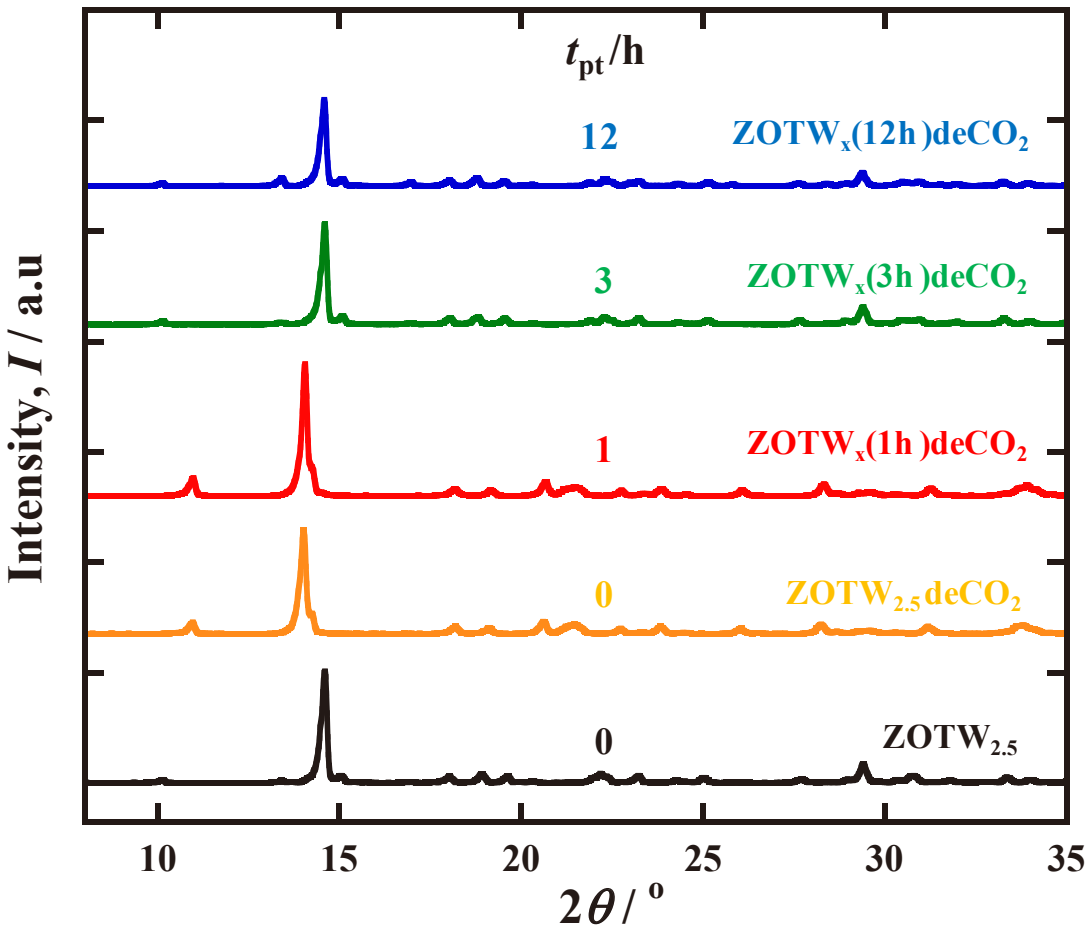

Figure 28. XRD patterns of $ZOTW_{2.5}$ and $ZOTW_x(t_{pt}h)$ (t_{pt}=0,1,3, 12) degassed after CO_2 adsorption.

The pore volume of $ZOTW_{2.5}deCO_2$ estimated by PLATON is 0.231 cm^3 g^{-1} (the porosity of 36.5 %) or Vs = 187 mg g^{-1}. The Vs value is much smaller than the experimental Vs values. Though the XRD pattern of $ZOTW_{2.5}deCO_2$ is certainly different from $ZOTW_{2.5}$, as shown in Figure 28, both analyzed crystal structures were quite similar, except for slight difference in the orientation of triazole. Thus, the high

adsorptivity of $ZOTW_{2.5}deCO_2$ cannot be explained by the structure obtained. Therefore, the crystal structure of $ZOTW_{2.5}deCO_2$ during N_2 adsorption should be different from that during XRD measurement to return to the initial structure almost reversibly, because the crystal was taken out from the adsorption system when the XRD was measured.

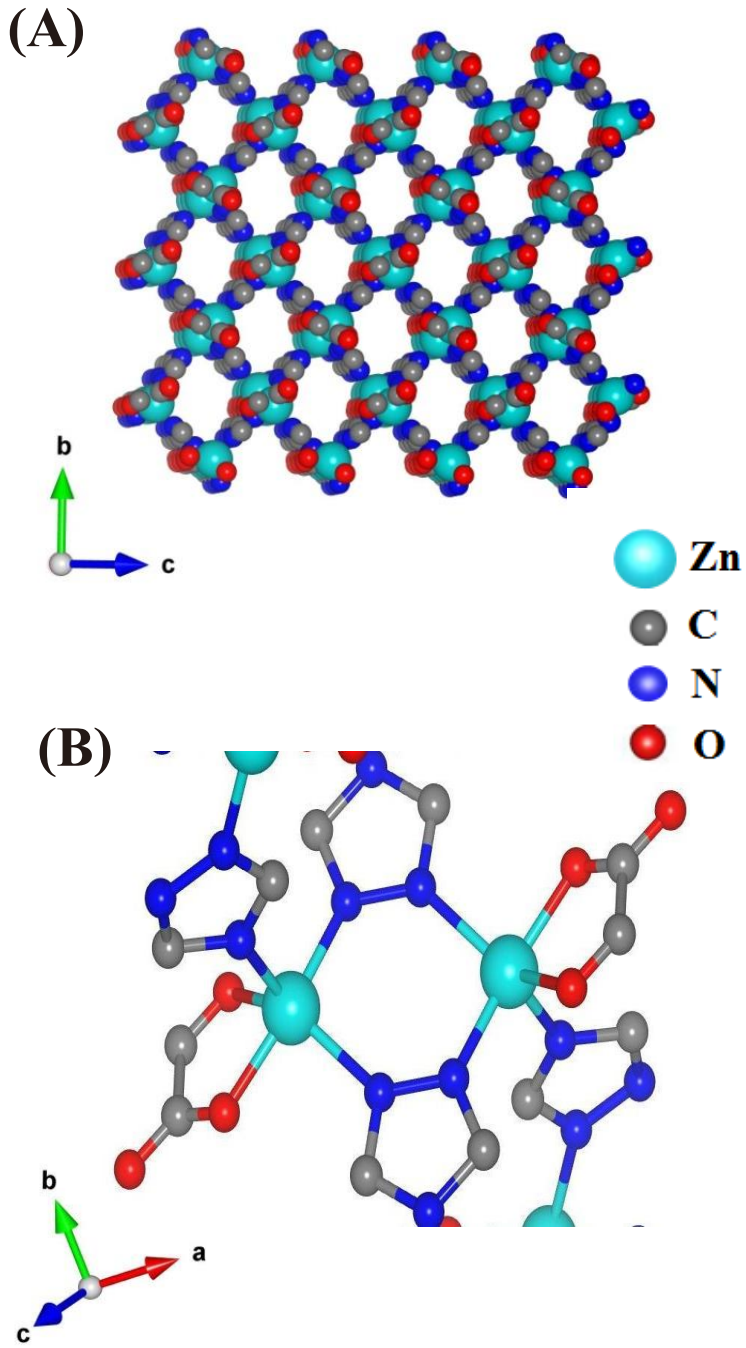

Figure 29. The crystal structure (A) and the local crystal structure (B) of $ZOTW_x(1h)deCO_2$ simulated by the Rietveld method.

2.4. Conclusion

I found a new micropore formation route via CO_2 adsorption on $ZOTW_x(\leq 2h)$ which is partially filled with water in micropores. N_2 adsorption on $ZOTW_x(\leq 2h)deCO_2$, degassed after CO_2 adsorption on $ZOTW_x(\leq 2h)$, was promoted by 5 times from 180 mg/g on $ZOTW_x(t_{pt}h)$ and $ZOTW_x(\geq 3h)deCO_2$ up to ca. 1000 mg/g. The interaction of CO_2 and H_2O molecules in micropores may lead to abundant micropore formation. The crystal structure specifies static pore size and volume, but adsorption amount depends on flexibility of frameworks. The large micropore volume of $ZOTW_x(\leq 2h)deCO_2$ may arise from faint changes in conformation such as the rotation of triazol rings and Zn-O bonds of oxalate ions in the flameworks. In order to proceed this technique, the micropore formation mechanism and stabilization method of micropores should be furthermore investigated.

Table 2. Structure analysis data for $ZOTW_{2.5.}$ and its refinement (cif file).

```
#======================================================================

# CRYSTAL DATA

#----------------------------------------------------------------------

data_VESTA_phase_1

_pd_phase_name                         'New structure'

_cell_length_a                         11.1408(18)

_cell_length_b                         7.94171(66)

_cell_length_c                         10.0605(17)

_cell_angle_alpha                      90

_cell_angle_beta                       128.288(9)

_cell_angle_gamma                      90

_symmetry_space_group_name_H-M         'P 21/c'

_symmetry_Int_Tables_number             14


loop_

_symmetry_equiv_pos_as_xyz

  'x, y, z'

  '-x, -y, -z'

  '-x, y+1/2, -z+1/2'

  'x, -y+1/2, z+1/2'


loop_

  _atom_site_label

  _atom_site_occupancy

  _atom_site_fract_x
```

_atom_site_fract_y

_atom_site_fract_z

_atom_site_adp_type

_atom_site_B_iso_or_equiv

_atom_site_type_symbol

Zn1	1.0	0.3074(4)	0.4660(4)	0.7696(4)	Biso 2.942294 Zn
C3	1.0	0.2832(17)	0.232(3)	0.497(2)	Biso 1.338449 C
O2	1.0	0.0977(13)	0.3267(13)	0.6589(15)	Biso 3.500025 O
O4	1.0	0.8520(13)	0.3785(14)	0.4358(15)	Biso 3.776303 O
N1	1.0	0.5024(15)	0.1473(15)	0.6339(18)	Biso 2.291392 N
O1	1.0	0.828(3)	0.200(3)	0.630(3)	Biso 32.008076 O
N2	1.0	0.3680(16)	0.3021(14)	0.6574(16)	Biso 0.386094 N
N3	1.0	0.3689(16)	0.1410(14)	0.4739(17)	Biso 0.578848 N
C4	1.0	-0.015(3)	0.418(2)	0.534(3)	Biso 1.139990 C
C6	1.0	0.5266(18)	0.221(2)	0.767(3)	Biso 1.000000 C
C1	1.0	0.928(3)	0.013(5)	0.371(3)	Biso 23.582052 C

loop_

_atom_site_aniso_label

_atom_site_aniso_U_11

_atom_site_aniso_U_22

_atom_site_aniso_U_33

_atom_site_aniso_U_12

_atom_site_aniso_U_13

_atom_site_aniso_U_23

Zn1	0.03726	0.03726	0.03726	0.00000	0.02308	0.00000
C3	0.01695	0.01695	0.01695	0.00000	0.01050	0.00000
O2	0.04433	0.04433	0.04433	0.00000	0.02747	0.00000
O4	0.04783	0.04783	0.04783	0.00000	0.02964	0.00000
N1	0.02902	0.02902	0.02902	0.00000	0.01798	0.00000
O1	0.40539	0.40539	0.40539	0.00000	0.25119	0.00000
N2	0.00489	0.00489	0.00489	0.00000	0.00303	0.00000
N3	0.00733	0.00733	0.00733	0.00000	0.00454	0.00000
C4	0.01444	0.01444	0.01444	0.00000	0.00895	0.00000
C6	-0.00001	-0.00001	-0.00001	0.00000	-0.00001	0.00000
C1	0.29867	0.29867	0.29867	0.00000	0.18506	0.00000

Table 3. Structure analysis data for ZOTW$_{2.5}$deCO$_2$ (cif file).

```
#======================================================================

# CRYSTAL DATA

#----------------------------------------------------------------------

data_VESTA_phase_1

_pd_phase_name                         'New structure'

_cell_length_a                         9.06318(92)

_cell_length_b                         9.76503(69)

_cell_length_c                         9.318(1)

_cell_angle_alpha                      90

_cell_angle_beta                       116.9161(74)

_cell_angle_gamma                      90

_symmetry_space_group_name_H-M         'P 21/c'

_symmetry_Int_Tables_number            14


loop_

_symmetry_equiv_pos_as_xyz

  'x, y, z'

  '-x, -y, -z'

  '-x, y+1/2, -z+1/2'

  'x, -y+1/2, z+1/2'


loop_

  _atom_site_label

  _atom_site_occupancy

  _atom_site_fract_x
```

_atom_site_fract_y

_atom_site_fract_z

_atom_site_adp_type

_atom_site_B_iso_or_equiv

_atom_site_type_symbol

Zn1	1.0	0.3114(7)	0.4488(5)	0.0551(8)	Biso	4.195937 Zn
O1	1.0	0.042(3)	0.071(3)	0.355(3)	Biso	4.206792 O
O2	1.0	0.193(3)	0.544(3)	0.180(3)	Biso	6.688343 O
N1	1.0	0.387(3)	0.142(3)	0.411(3)	Biso	3.165324 N
N2	1.0	0.376(3)	0.2811(19)	0.215(3)	Biso	0.716940 N
N3	1.0	0.517(3)	0.117(2)	0.367(3)	Biso	3.410816 N
C1	1.0	0.527(4)	0.202(4)	0.249(4)	Biso	3.598029 C
C2	1.0	0.259(3)	0.267(3)	0.288(4)	Biso	3.061800 C
C3	1.0	0.077(5)	0.531(5)	0.111(5)	Biso	8.032329 C
O4	1.0	1.119(5)	0.894(3)	1.112(6)	Biso	43.325119 O

loop_

_atom_site_aniso_label

_atom_site_aniso_U_11

_atom_site_aniso_U_22

_atom_site_aniso_U_33

_atom_site_aniso_U_12

_atom_site_aniso_U_13

_atom_site_aniso_U_23

Zn1	0.05314	0.05314	0.05314	0.00000	0.02405	0.00000
O1	0.05328	0.05328	0.05328	0.00000	0.02412	0.00000
O2	0.08471	0.08471	0.08471	0.00000	0.03835	0.00000
N1	0.04009	0.04009	0.04009	0.00000	0.01815	0.00000
N2	0.00908	0.00908	0.00908	0.00000	0.00411	0.00000
N3	0.04320	0.04320	0.04320	0.00000	0.01956	0.00000
C1	0.04557	0.04557	0.04557	0.00000	0.02063	0.00000
C2	0.03878	0.03878	0.03878	0.00000	0.01756	0.00000
C3	0.10173	0.10173	0.10173	0.00000	0.04605	0.00000
O4	0.54872	0.54872	0.54872	0.00000	0.24840	0.00000

Chapter 3 Magnetic field control of micropore formation in $[Zn_2(Oxac)(Taz)_2].(H_2O)_x$

3.1. Introduction

Porous coordination polymers (PCPs) are a new class of porous crystalline materials that have extremely high porosity and selective adsorptivity for guest molecules [46-49]. Gas storage capacity in PCPs was promoted by introducing open metal sites [52], increasing surface area [54], and modifying pores with functionalized organic linker [62]. The gate-controlled adsorption was found that the latent pores of flexible PCPs opened above a critical pressure [47,57]. Such flexible PCPs were brought about after desolvation. Amounts of solvent surrounded by frameworks of PCPs are very important for formation of latent pores and their flexibility as well as pore volume and adsorptivity.

We reported a new route for micropore formation of one of PCPs, $[Zn_2(Oxac)(Taz)_2].(H_2O)_{2.5}$ referred to $ZOTW_{2.5}$; i.e., the CO_2-assisted micropore formation via water-assisted CO_2 adsorption on $ZOTW_x$. Although the as-synthesized $ZOTW_{2.5}$ pretreated gently had little open micropores because of some water left, the water assisted adsorption of CO_2 to bring about formation of abundant open micropores after vacuum-degassing.

Magnetic fields (H/T) drastically modify the structures and properties of materials, especially colloidal systems [65-70]. Homogeneous magnetic fields affect them thermodynamically via magnetic energy, $(1/2)\chi H^2$, which may induce the magnetic orientation, phase transition, etc. Magnetic field gradient also brings about magnetic force, which causes convection, mass-transport, concentration change, etc. For molecules having lower symmetry than cubic symmetry, the magnetic susceptibility is anisotropic (dependent on direction), and the magnetic energy is anisotropic (different by direction). In this study, magnetic field control of pore formation of a PCP comprised of metal ions and magnetically anisotropic ligands was investigated. $ZOTW_{2.5}$ was synthesized under magnetic fields of up to 6 T and their morphology of crystals, crystal structure, size and properties of micropores were examined.

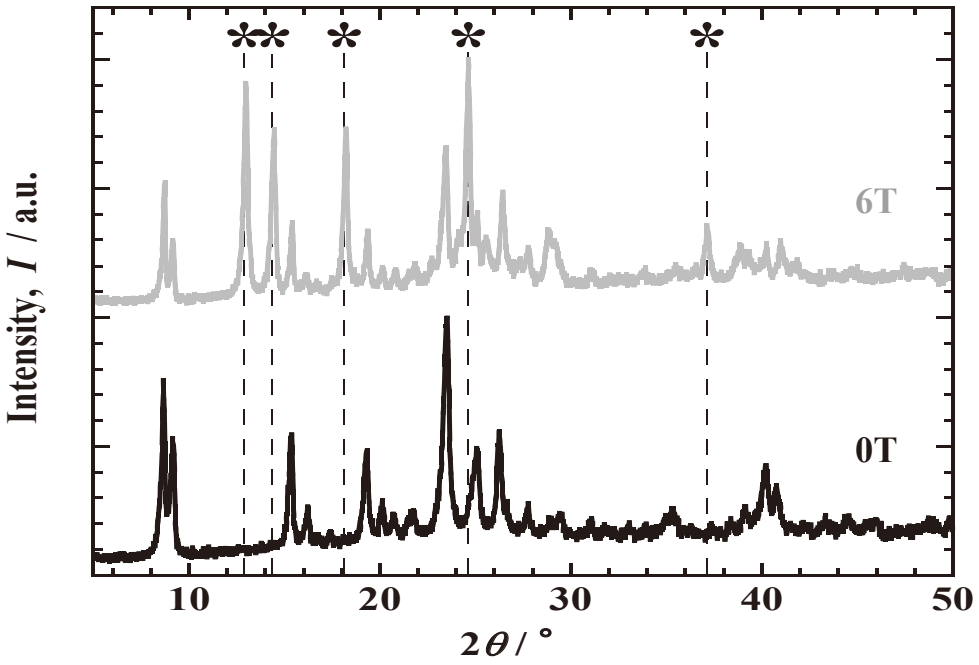

Figure 30. Powder X-ray diffraction patterns of Cu/pyz/pzdc complexes prepared at 298 K under 0 T and 6 T [27].

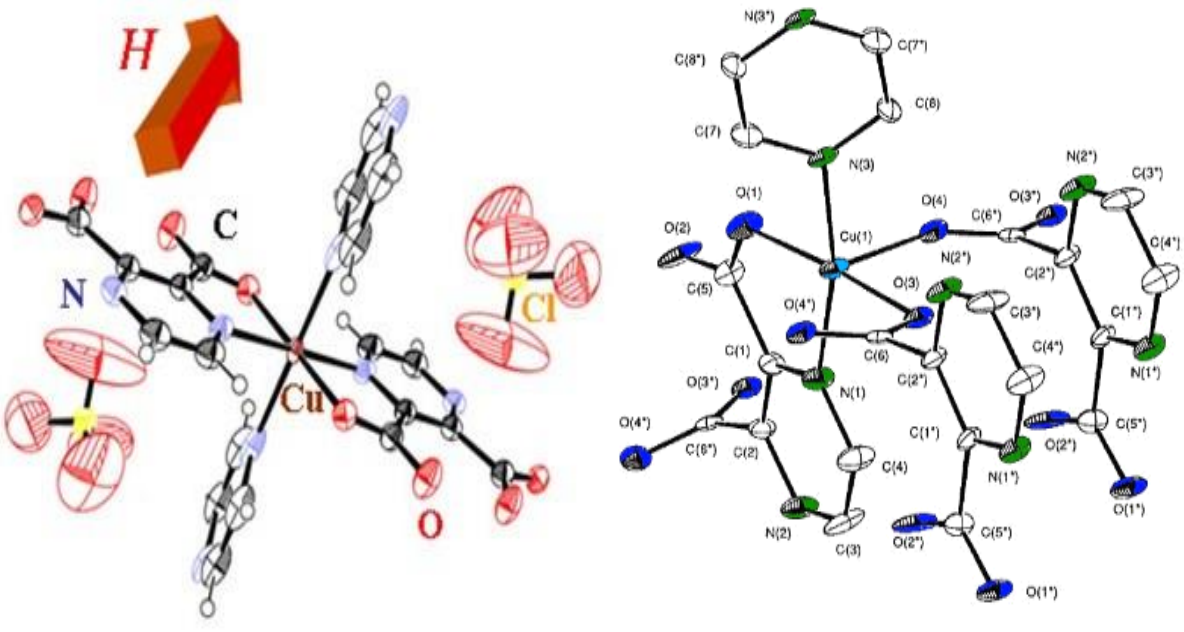

6T **0T**

Figure 31. Crystal structure of Cu/pyz/pzdc complexes prepared at 298 K under 0 T and 6 T [27].

3.2. Experimental Section

0.4g of $Zn_5(CO_3)_2(OH)_6$, 0.4g of $H_2C_2O_4$, and 1.4g of 1,2,4-triazole were added to a mixed solvent of 12mL of methanol and 2mL of distilled water. The dispersion was transferred to a Teflon cell which was set in an autoclave vessel made of non-magnetic stainless steel (SUS316). The vessel was put in the center of magnetic fields (2, 4, and 6T) of a JASTEC JMTD-6T150E1 superconducting magnet as shown in Fig. 32, and heated in the homogeneous magnetic field region within ±3 % at 453 K for 12 h. After cooling the system to room temperature under magnetic fields, the prepared crystals were filtered and washed with the solvent, followed by drying them in air at room temperature. The prepared crystals were characterized by a Rigaku Multiflex X-ray diffractometer (XRD) with Cu Kα and observed by a JEOL JSM-7600F scanning electron microscope (SEM). The crystal structure was determined by the Rietveld method using RIETAN-FP program.

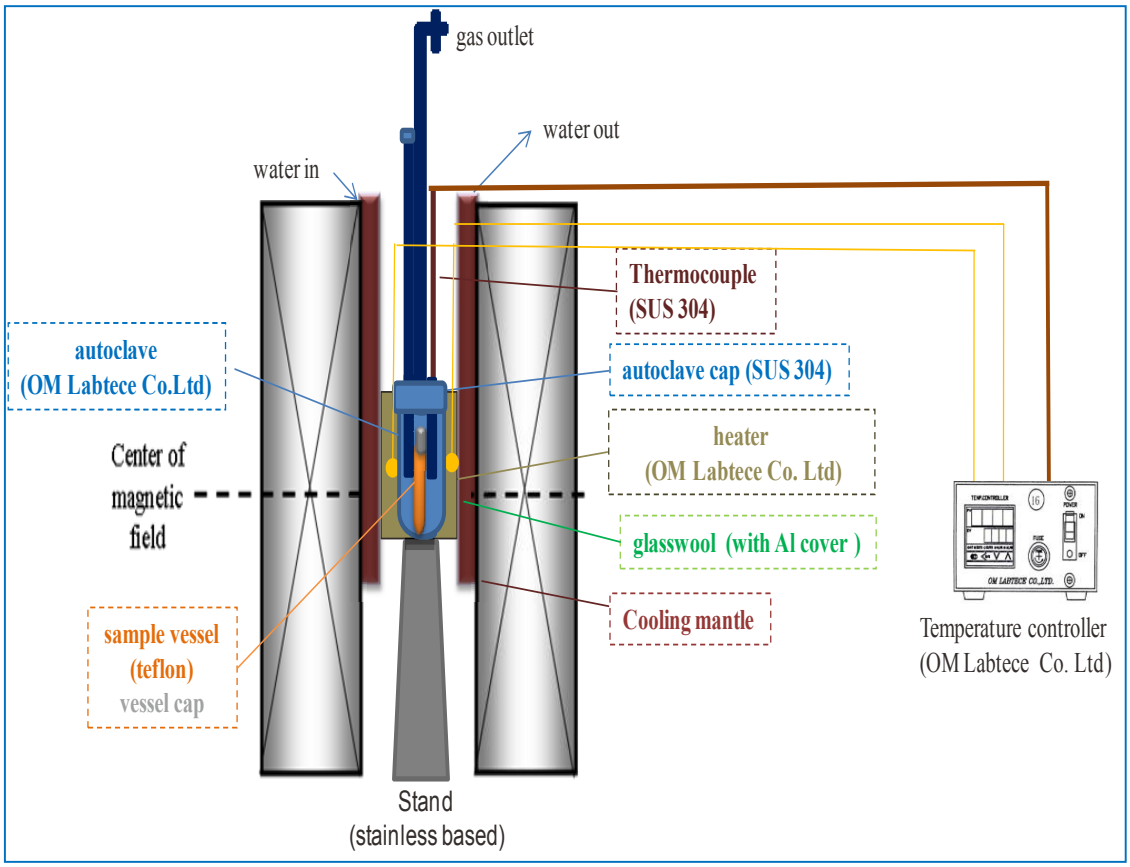

Figure 32. Synthesis method and design of $[Zn_2(Oxac)(Taz)_2]\cdot(H_2O)_{2.5}$, $ZOTW_{2.5}$ in magnetic fields.

Amount of solvent included in PCPs was examined gravimetrically at 383 K as a function of heating time. The elementary analysis of C, H, and N was carried out with a Flash EA1112 elementary analyzer. N_2 and CO_2 adsorption were measured at 77 and 303 K, respectively, by a custom-made volumetric adsorption system after pretreatment at 383 K and 1 mPa for various times, t_{pt}. When second N_2 adsorption was carried out after CO_2 adsorption, the sample used for CO_2 adsorption was degassed at 298 K and 10 mPa for 30 min before the N_2 adsorption.

3.3. Results and Discussion

The previous chapter showed that the crystal prepared at 0 T (zero field) was $[Zn_2(Oxac)(Taz)_2]\cdot(H_2O)_{2.5}$, referred to $ZOTW_{2.5}$, and that its crystal structure was determined P_{21}/a by the Rietveld method. The Zn^{2+} ion in $ZOTW_{2.5}$ had 5 coordination number comprising three Taz molecules and an Oxac molecule. The XRD patterns of white crystals prepared at H/T = 2, 4, and 6, referred to $ZOTW_x(H)$, were similar to that of zero field (Figure 33). The reproducibility only at around 2 T was insufficient. Although the crystal structures estimated by the EXPO 2014 program were monoclinic at 0 T and triclinic under magnetic fields of up to 6 T (Table. 4), the structural change was delicate, as the Rietveld analysis suggested a similar structure to that for zero-field sample. Also, the composition of the crystals estimated by the elementary analysis was unchanged by applying any magnetic fields, except for water (x=1.9–2.3). However, magnetic fields more than 2 T induced the morphology change of irregular agglomerates at zero field to rectangular-prism crystals having smooth surfaces and larger size, as seen in the SEM images (Figure 34). Such magnetic field effects may arise from depression of the nucleation process on crystal surfaces. The transport of reactants due to convection and/or diffusion may be depressed because of the gradients in magnetic field and magnetic susceptibility of the solution. Thus, the crystal growth should be slow to make their inner as well as outer surfaces smooth. Moreover, it is known that magnetic fields may interact with water [68] and thus may affect crystal formation via hydrated reactants [70].

Figure 35 shows adsorption isotherms of N_2 on $ZOTW_x(H)(t_{pt}/h)$ pretreated at 383 K for t_{pt}/h. The micropores of $ZOTW_x(0)(\leq 3h)$ pretreated within 3 h were closed with water, as little amount of N_2 adsorbed. Pretreatment over 3 h made $ZOTW_x(0)(>3h)$

adsorb N_2, and gave Type I adsorption isotherms, indicating open micropore formation due to water removal. On the other hand, applying magnetic fields more than 2 T to the reaction solutions, as-synthesized ZOTW$_x$(*H*)(0h)s (H/T≥2) adsorbed abundant amount of N_2 at low pressure even without pretreatment.

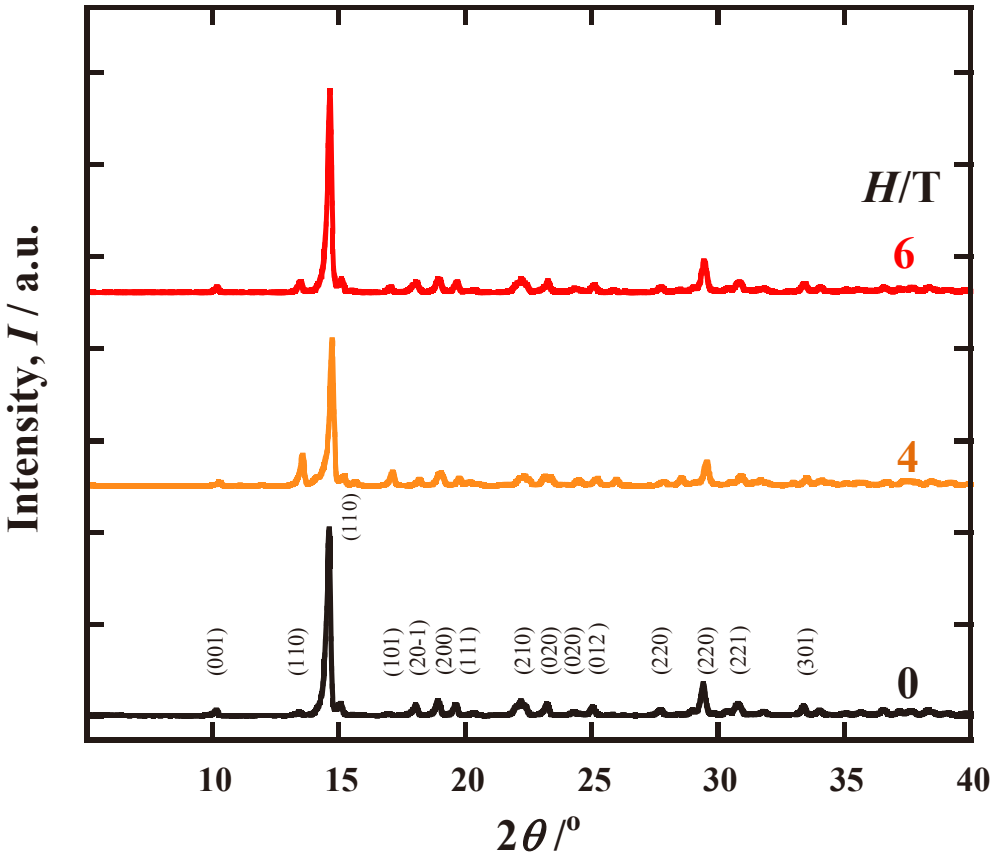

Figure 33. The XRD patterns of as-synthesized ZOTW$_x$(*H*)(0h) prepared at *H*/T = 0, 4, and 6.

Table 4. Summary of crystal parameters by using EXPO 2015 Analysis

No	PCPs Crystal	a (Å)	b (Å)	c (Å)	α (°)	β (°)	γ (°)	Crystal System
1	Zn-oxac-Taz 0T	10.025	7.970	9.339	90.000	110.660	90.000	Monoclinic
2	Zn-oxac-Taz 4T	11.032	14.583	8.351	99.276	103.555	85.854	Triclinic
3	Zn-oxac-Taz 6T	11.921	10.115	9.516	93.898	111.112	81.034	Triclinic

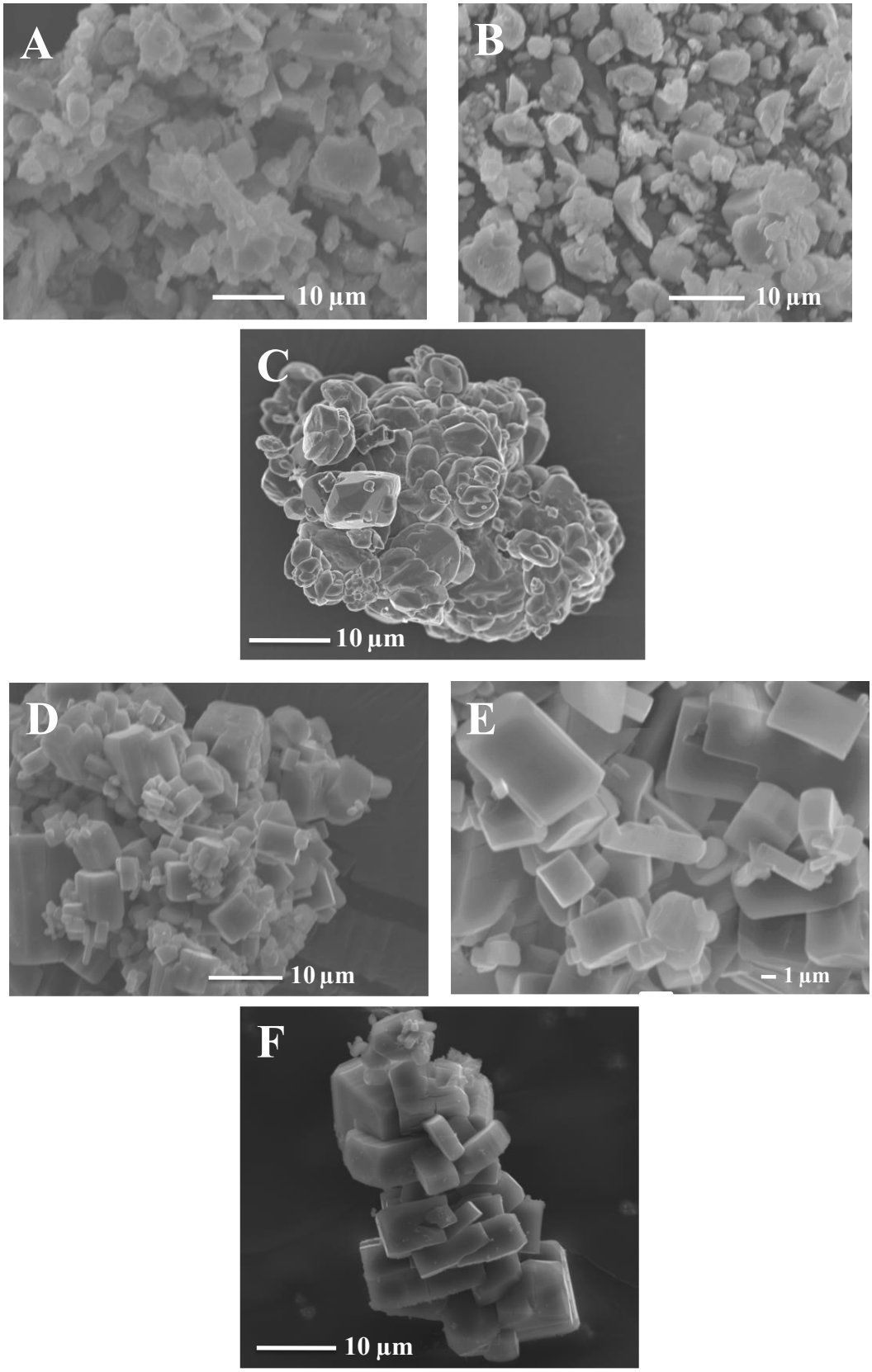

Figure 34. The SEM images of ZOTW$_x$(0)(0h), (A, B, C) and ZO1W$_x$(6)(0h), (D, E, F)

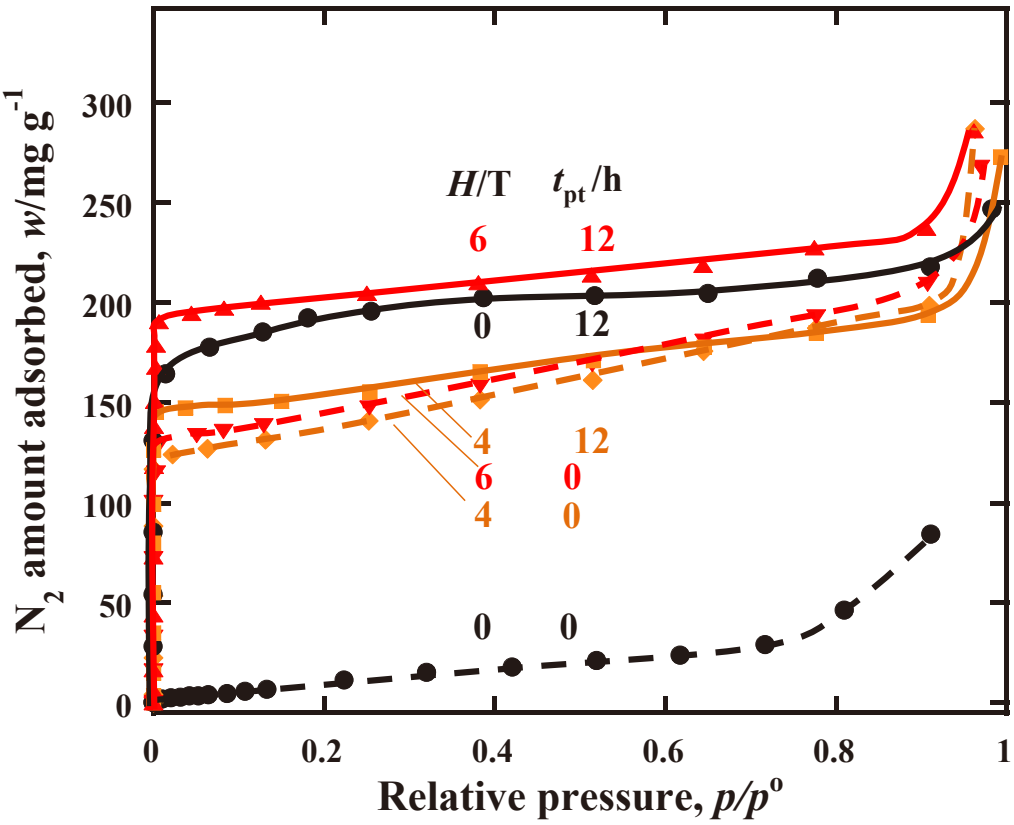

Figure 35. N_2 adsorption isotherms (solid lines) for $ZOTW_x(0)(0h)$, $ZOTW_x(4)(0h)$, and $ZOTW_x(6)(0h)$ prepared at 0, 4, and 6 T, respectively. Broken lines are N_2 adsorption isotherms for $ZOTW_x(0)(12h)$ and $ZOTW_x(6)(12h)$ having open micropores. The isotherms were measured at 77 K after ZOTs were pretreated at 383 K for various times, t_{pt}/h.

Figure 36 summarizes the dependence of pore volumes of $ZOTW_x(H)$s (H/T = 0~6) on pretreatment time (t_{pt}/h). The pore volumes were estimated by the DR plots. Higher magnetic fields than 2 T promoted open pore formation due to depression of water inclusion in crystal-growing. This suggests that the micropore walls or frameworks of $ZOTW_x(H)$ should be hydrophobic. Figure 37 shows water loss of $ZOTW_x(H)(0h)$s stored in air as a function of time kept at 298 K for 10 min and subsequently at 383 K. In the first 10 min, water included in $ZOTW_x(4)(0h)$ and $ZOTW_x(6)(0h)$, which will be removed at 383 K, was almost removed at 298 K, but hardly in $ZOTW_x(0)(0h)$ from which water was evolved during heating at 383 K. The water loss decreased with increase in magnetic field intensity, suggesting promotion of the hydrophobicity of

micropores due to magnetic fields. The water-frameworks interactions in ZOTW$_x$(*H*)s are much weaker than the strong interaction between water and micropores of as-synthesized ZOTW$_{2.5}$(0) prepared at zero field.

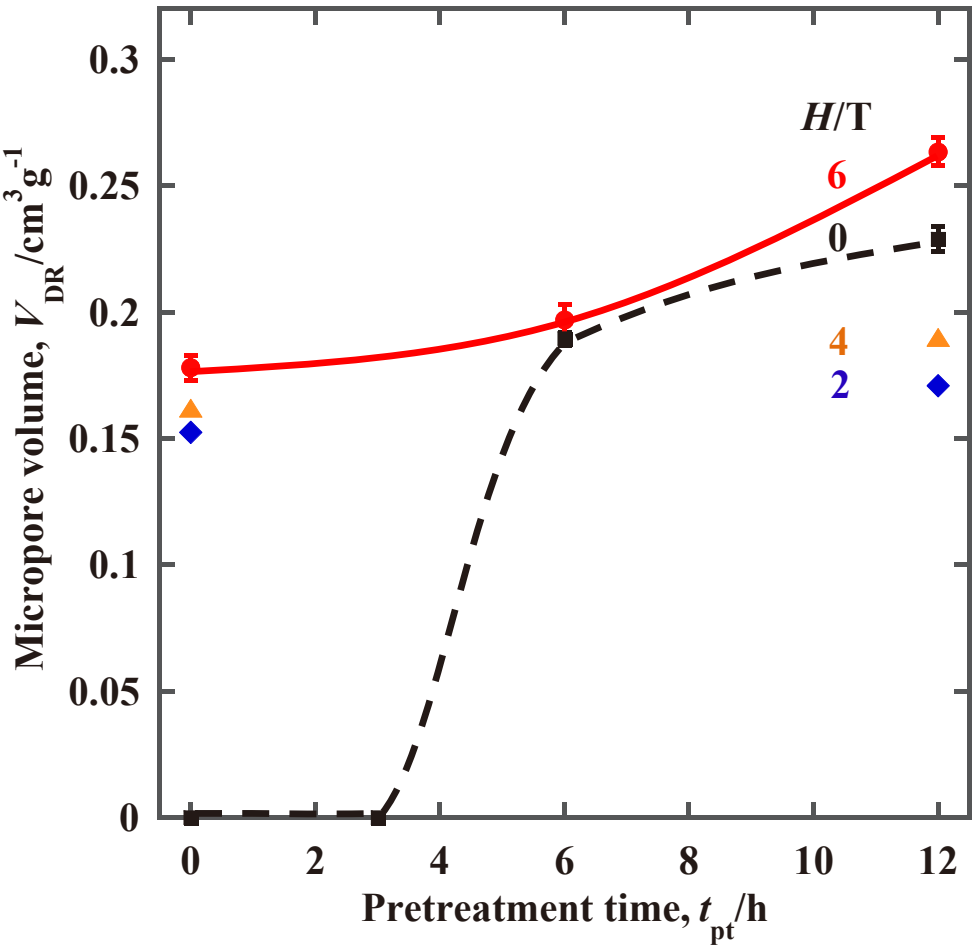

Figure 36. Dependence of micropore volume of ZOTW$_x$(*H*) prepared at *H*/T = 0, 2, 4, and 6 on pretreatment time, t_{pt}/h.

It is noteworthy that all N_2 adsorption isotherms for ZOTW$_x$(*H*)s prepared under magnetic fields, irrespective of the degree of pretreatment, and also ZOTW$_x$(*H*)(0h)deCO_2 (Fig.39) were rectangular Type I having a sharp break point, which was different from the round break point of Type I isotherm for zero-field sample ZOTW$_{2.5}$(0). The sharpness in the isotherms demonstrates a narrow pore size distribution. Such uniform size in micropores should be attributed to magnetic field

effects, which may be consistent with slow crystal growth under magnetic field, as suggested by the morphology change.

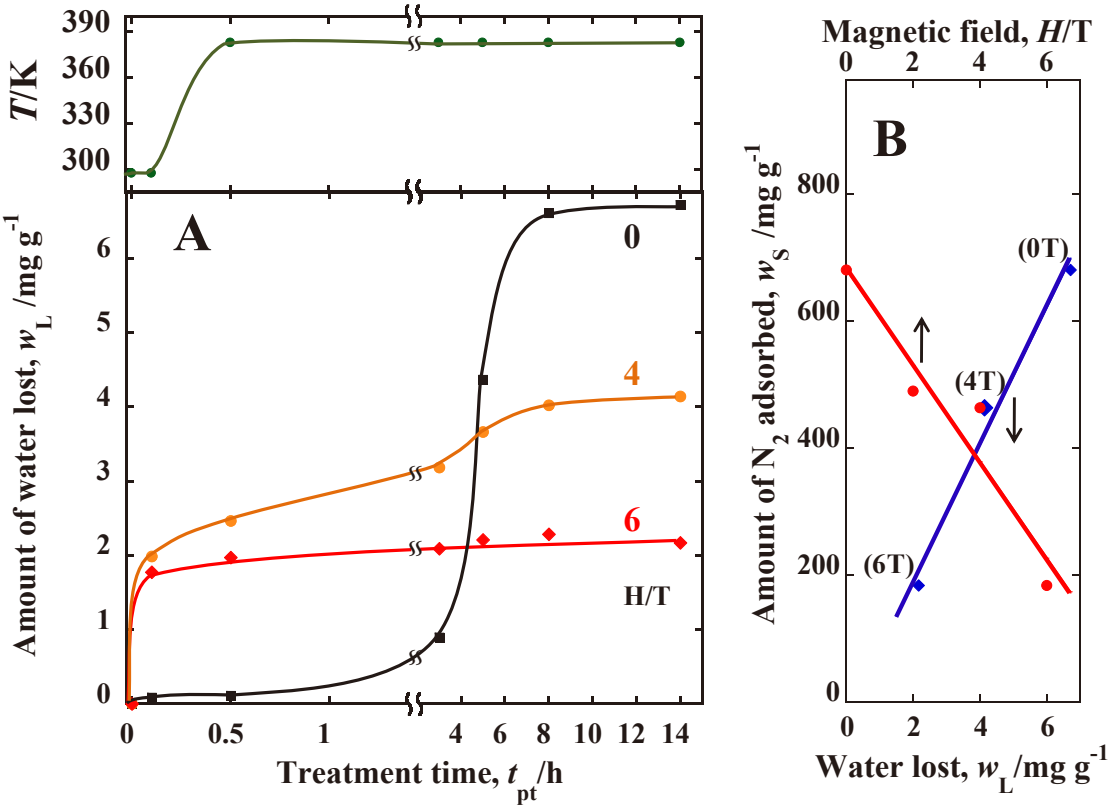

Figure 37. **A.** Amount of water lost from as-synthesized ZOTW$_x$(H)(0h) prepared at H/T = 0, 4, and 6 (lower) by heating at 298 K in first 10 min and subsequently at 383 K (upper). **B.** The relationship between amount of water lost from ZOTW$_x$(H)(0h) (Fig.36A) and saturation amount of N_2 adsorbed on ZOTW$_x$(H)(0h)deCO_2 (Fig.38).

The open micropores of ZOTW$_x$(6)(0h) and ZOTW$_x$(6)(12h) adsorbed CO_2 at 303 K up to W /mg g^{-1} = 140 at 700 Torr (Figure 38). The adsorption amounts of ZOTW$_x$(6)s prepared at 6 T were much more than that (110 mg g^{-1} at 700 Torr) of ZOTW$_x$(0)(12h) even without pretreatment. When ZOTW$_x$(H)s were not pretreated, adsorption amount of CO_2 increased with increase in magnetic field intensity at CO_2 pressure lower than 400 Torr. The amounts of CO_2 adsorbed on ZOTW$_x$(2)(0h) and ZOTW$_x$(4)(0h) seems to be too little compared with their open-pore volumes. A CO_2 molecule is larger in averaged size than an N_2 molecule and also may interact with water in micropores to be prevented

from diffusing. At higher pressure CO_2 was adsorbed much more, presumably by pseudo-high pressure in micropores.

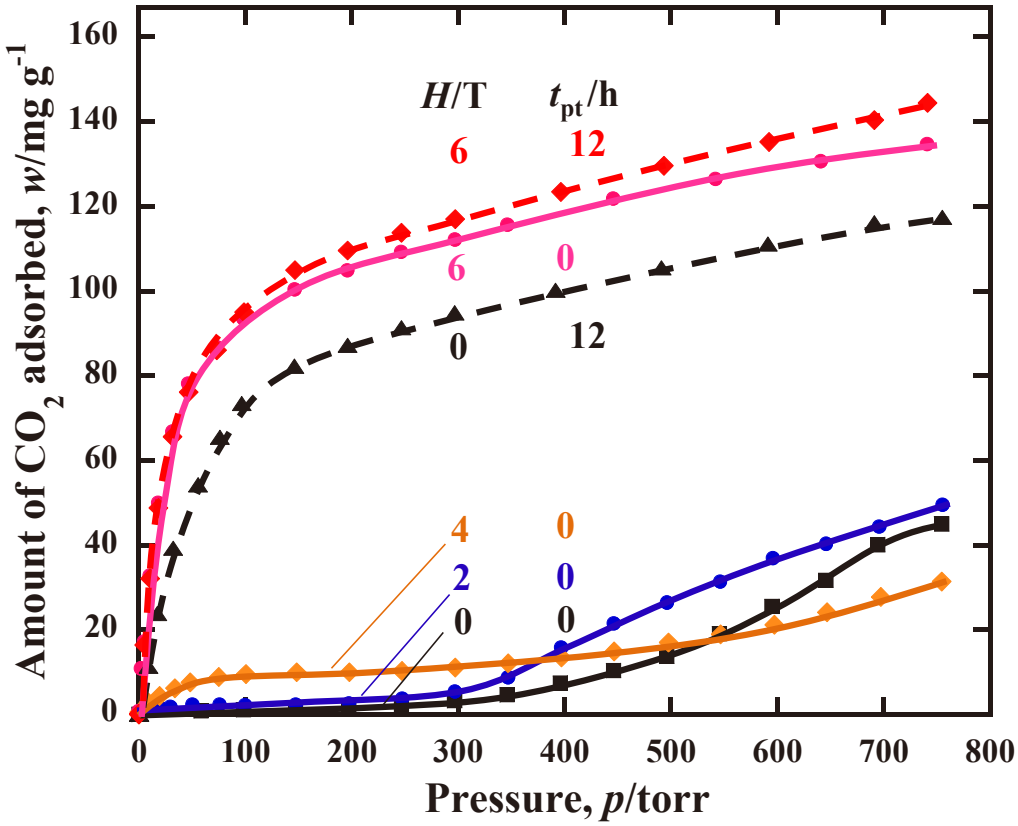

Figure 38. CO_2 adsorption isotherms measured at 303K for $ZOTW_x(H)(0h)$ (H/T = 0, 2, 4, and 6) and $ZOTW_x(H)(12h)$ (H/T = 0 and 6).

In the previous chapter, such high CO_2 adsorptivity for micropores closed with water was ascribed to a specific species formed by CO_2 and cage comprising H_2O and frameworks. Though the amount of CO_2 occluded in closed micropores of $ZOTW_x(0)(1h)$ was not so much still, the saturation amount of N_2 increased remarkably from 200 to 1000 mg g^{-1}, by degassing the CO_2-adsorbing $ZOTW_x(1h)$ at 298 K for 30 min. This new route for micropore formation of PCPs was ascribed to structural changes of the crystal due to the decomposition of the specific species. Such assumption also seems to be applicable to the results in Figure 37 and Figure 38. The micropores of $ZOTW_x(H)(0h)$s may be hydrophobic and thus contains less amount of water than $ZOTW_x(0)(0h)$ (Fig. 37A). Therefore, amounts of the specific species formed by introducing CO_2 should be reduced by magnetic fields applied in $ZOTW_x(H)$ preparation.

Thus, the new pore formation via the decomposition of the specific species should be depressed with increase in magnetic field intensity. Figure 39 indicates the case; the saturation amount of N_2 adsorbed on ZOTW$_x$(*H*)(0h)deCO_2 increases with increase in water content in ZOTW$_x$(*H*)(0h), as shown in Fig.37B. The adsorption isotherms again are rectangular Type I, indicating uniformity in the micropore size of around 0.7 nm.

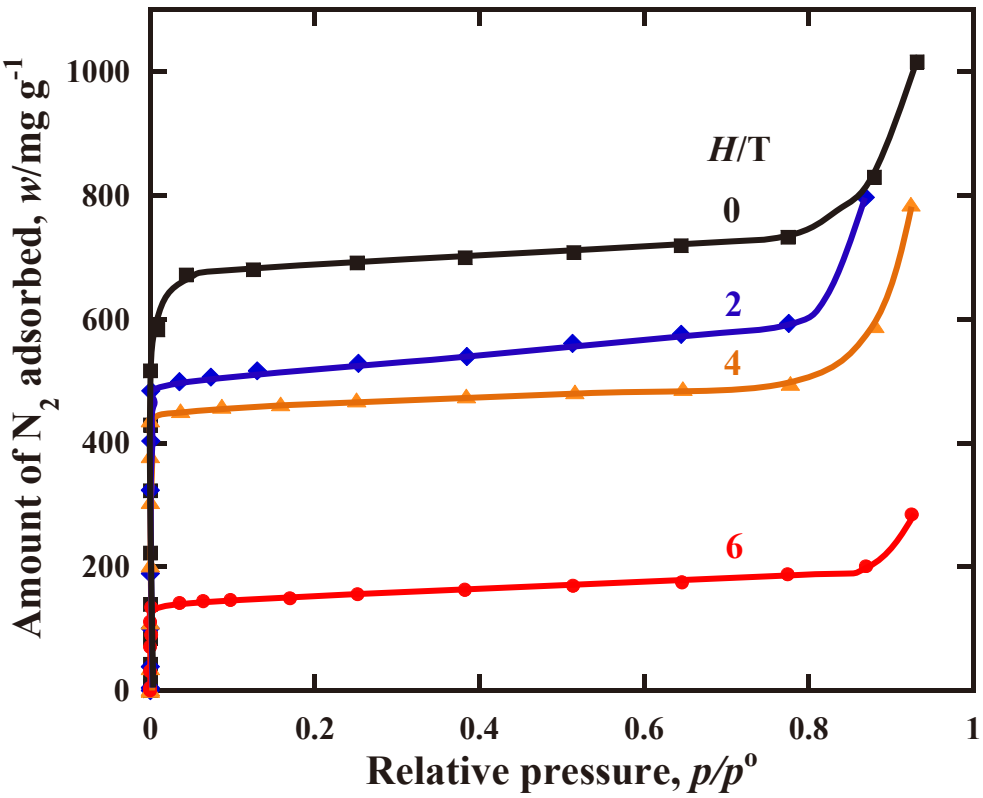

Figure 39. N_2 adsorption isotherm at 77 K for ZOTW$_x$(*H*)(0h)deCO_2 (*H*/T = 0, 2, 4, and 6), which were degassed at 298 K after CO_2 adsorption (Fig. 36).

3.4. Conclusion

In conclusion, magnetic fields higher than 2 T affected the structure and properties of micropores in ZOTW$_x$(*H*)s as well as their morphology, when they are applied to the reaction solutions. The micropores of ZOTW$_x$(*H*) crystals may become hydrophobic and uniform in size. Utilizing the CO_2-assisted pore formation, the promotion of hydrophobicity due to magnetic fields was confirmed. Magnetic fields may control the volume, size and its uniformity, and hydrophobicity of micropores.

Chapter 4. Summary and Outlook

These results established a new pore properties of porous coordination polymers $[Zn_2(Oxac)(Taz)_2].(H_2O)_{2.5}$ that created by CO_2 molecule interaction with frameworks to form the secondary pore with remarkable pore properties. As generally, longer pretreatment removed solvent to make open pores, however CO_2 molecules may exchange solvent molecules inside the pore to produce secondary pores.

The crystal structure of as-synthesized PCP, was estimated by the Rietveld method. The three dimensional frameworks built from the pillaring of Zn-triazolate layers by the oxalate groups. The oxalate ligands bind to the zinc in a bidentate mode through two oxygen atom from different carboxylate groups. The triazolate ligand bind to trigonal bipyramidal zinc centers through the three N-atoms of the ring explores new design of PCPs as $Zn_2(C_2O_4)(C_2N_3H_2)_2.(H2O)_{2.5}$ or Zn-oxac-Taz PCP with triazolate ligands without amine groups presence which promoted significant N_2 amount adsorption isotherms and also available space to accept carbon dioxide molecules. If compare with others $Zn_2(C_2O_4)(C_2N_4H_3)_2.(H_2O)_{0.5}$ or Zn-oxac-ATaz PCP which have amine groups in ligands structure, no space observed for nitrogen adsorption isotherms even could capture CO_2 molecules due to their amine groups presence inside the pore interacted with CO_2 molecules.

CO_2 was adsorbed at 303 K in sigmoid on non-porous $ZOTW_x$(0~2h) and in Langmuir-type on $ZOTW_x$(≥3h) to reach the adsorption amount of 120 mg/g at 700 Torr. N_2 adsorption on only $ZOTW_x$(0~2h) degassed after CO_2 adsorption was enhanced up to 1000 mg/g in *V*s. The interaction of CO_2 and H_2O molecules in micropores of $ZOTW_x$ may lead to specific CO_2 hydrate formation to produce new micropores with their removal in degassing. A new pore formation route via water-assisted CO_2 adsorption on $ZOTW_{2.5}$. The crystal structure specifies static pore size and volume, but adsorption amount depends on the dynamical sizes or flexibility of molecules and frameworks.

$Zn_2(C_2O_4)(C_2N_3H_2)_2.(H2O)_{2.5}$ also were synthesized under magnetic fields up to 6T. Even no significant different XRD pattern of OT, 4T and 6T crystals, however morphology of crystal changed from disorder shape at 0T to cubic shape at 6T with smoothly surface. PCP prepared at 0T could adsorb nitrogen after pretreatment at 110 ^{0}C over 3 hours. On the other hand, 4T and 6T crystals adsorbed nitrogen even without any

pretreatment. It is suggesting that PCPs synthesis under magnetic fields made the latent pores opened. Especially for 4T crystal, after 12 h pretreatment nitrogen adsorbed lower than 0T and 6T, indicate the smaller pore formed even pores opened without heating of pretreatment. If refer to XRD patterns, it is related to low intensity changed of XRD peak in 4T crystals.

Overall, some interesting strategy to enhance carbon dioxide capture on PCP were - successfully established from new flexibility $Zn_2(Oxac)(Taz)_2.(H_2O)_{2.5}$. Upon carbon dioxide adsorption isotherms, this PCP created the new pore properties. And synthesis under magnetic fields also generated the new pore properties which formed porous material with latent open pores. Nitrogen and carbon dioxide could penetrate inside the frameworks even without any pretreatment. Magnetic fields higher than 2 T affected the structure and properties of micropores in $ZOTW_x(H)$s as well as their morphology, when they are applied to the reaction solutions. The micropores of $ZOTW_x(H)$ crystals may become hydrophobic and uniform in size. Utilizing the CO_2-assisted pore formation, the promotion of hydrophobicity due to magnetic fields was confirmed. Magnetic fields may control the volume, size and its uniformity, and hydrophobicity of micropores.

References

1. Borislav D. Zdravkov; Jirı J. Cermak; Martin Sefara; Josef Jank, Central European Journal of Chemistry, Pore Classification in the characterization of porous materials: A. Perspective.CEJC 5(2) **2007**, 385–395 .
2. Blaine W. Assay, Shock wave science & technology, Reference library, Vol. 5 Spinger, **2010.**
3. Rouquerol, F; Rouquerol, J; Sing, K. S. W.; Llewellyn, P.; Maurin, G., Adsorption by Powders and Porous Solids; Principles, Methodology and Applications. Second edition, **2014**.
4. Mineral Commodity Summaries: Zeolite Natural, US Geological Survey, Reston, Virginia, **2012**.
5. Stephen H, et al, *J. Matter Chem*, **2006**, 16, 2464.
6. Choudhary V; Anju G, Carbon nanotubes – polymer nanocomposites, Indian Institute of Technology Indian, **2017**.
7. Kitagawa, S.; Kitaura, R.; Noro, S., *Angew. Chem. Int. Ed*. **2004**, *43*, 2334.
8. Omar K. Farha; Joseph T. HUPP. Accounts of Chemical Research. **2010**, 43, 1166-1175.
9. Horike, S.; Shimomura, S.; Kitagawa, S., Soft Porous Solids. *Nat. Chem*. **2010**, *1*, 695-704.
10. Jesse L.C. Rowsell; Omar M. Yaghi, *Microporous and Mesoporous Materials*. **2004**, *73*, 3 -14.
11. Ryan J. Kuppler, et al, *Coordination Chemistry Reviews*. **2009**, *253*, 3042-3066.
12. Yilmaz, B.; Trukhan, N.; Müller, U., *Chin. J. Catal*. **2012**, *33*, 3–10.
13. Noro, S.; Kitagawa, S.; Akutagawa,; T.; Nakamura, T., *Prog. Polym. Sci*. **2009**, *34*, 240-279.
14. Demazeau, G., *J. Mater. Chem*. **1999**, *9*, 15–18.
15. Laye, R.H.; McInnes, E.J.L, *Eur. J. Inorg. Chem*. **2004**, 2811–2818.
16. Rabenau, A., *Angew. Chem. Int. Ed*. **1985**, *24*, 1026–1040.
17. Birkholz, M., Thin Film Analysis by X-Ray Scattering, WILEY-VCH Verlag GmbH & Co. KGaA, Weinheim. **2006.**
18. Cavka, J.H.; Jakobsen, S.; Olsbye U.; Guillou N.; Lamberti C.; Bordiga S. and Karl Lillerud, K.P., *J. Am. Chem. Soc.* **2008**, *130*, 13850–13851.

19. Altomare, A.; Cuocci, C.; Giacovazzo, C.; Moliterni, A.; Rizzi, R.; Corriero, N.; Falcicchio, A., *J. Appl. Cryst*. **2013**, *46*, 1231.
20. Oszla'nyi, G. & Suto, A, The charge flipping algorithm, Acta Crystallographica, **2008**, A64, 123-134
21. Felipe G.; Fernando J.; Uribe-Romo; David K.B.; Hiroyasu F.; Liao L.; Rui C.; Xiangfeng D.; Michael O. K.; and Omar M. Y., *Chem. Eur. J*. **2012**, *18*, 10595 – 10601
22. Baerlocher C.H.; Lynne B. McCusker, Olson D. H., Atlas of Zeolite Frameworks Type, sixth Revised Edition, Christian Laboratory of Crystallography ETH Zurich 8093 Zurich, Switzerland ; Department of Chemistry and Chemical Biology Rutgers University Piscataway, NJ 08854, USA. Structure Commission of the International Zeolite Association by Elsevier, **2007**.
23. Sun, Qian; Yerino, Christopher D.; Zhang, Yu; Cho, Yong Suk; Kwon, Soon-Yong; Kong, Bo Hyun; Cho, Hyung Koun; Lee, In-Hwan; Han, Jung, *J of Crystal Growth*, **2009**, *311*, 3813-3816.
24. Xie, D., Baerlocher, Ch. & McCusker, L. B. , *J. Appl. Cryst*. **2011**, *44* ,1023–1032.
25. Gandara, F, and Bennet, T. D. , *IUCrJ*. **2014**, *1*, 563-570
26. Dunlap, M.; Adaskaveg, J. E., Introduction to the scanning electron microscope theory, practice and procedure, Facility for Advanced Instrumentation, U.C. Davis, **1997**.
27. Sakaguchi, A.; Hamasaki, A.; Ozeki, S., *Chem. Lett*. **2012**, *41*, 342.
28. Cui, H.B.; Wang, Z.M.; Takahashi; K.,Okano, Y.; Kobayashi, H.; Kobayashi, A., *J. Am. Chem. Soc*. **2006**.*128*, 15074 – 15075.
29. Cui, H.; Zhou, B.; Long, L.S.; Okano, Y.; Kobayashi, H.; Kobayashi, A, *Angew. Chem. Int. Ed*. **2008**, *47*, 3376-3380.
30. Jain, P.; Dalal, N.S.; Toby, B.H.; Kroto,H.W.; Cheetham, A.K, *J. Am.Chem. Soc*. 2**008**. *130*, 10450-10451.
31. Jain, P.; Ramachandran, V.; Clark, R.J.; Zhou, H.D.; Toby, B.H.; Dalal, N.S.; Kroto, H.W.; Cheetham, A.K, *J. Am.Chem. Soc.* **2009**, *131*, 13625-13626.
32. Ye, H.Y.; Fu, D.W.; Zhang, Y.; Zhang, W.; Xiong, R.G.; Huang, S.D, *J. Am. Chem. Soc.* **2009,** *131*, 42-43.

33. Deng, H.X.; Doonan, C.J.; Furukawa, H.; Ferreira, R.B.; Towne, J.; Knobler, C.B.; Wang, B.; Yaghi, O.M. *Science*. **2010**, *327,* 846-850.
34. Fukushima, T.; Horike, S.; Inubushi, Y.; Nakagawa, K.; Kubota, Y.; Takata, M.; Kitagawa, S., *Angew. Chem. Int. Ed*. **2010**, *49*, 4820-4824.
35. Botas, J.A.; Calleja, G.; Sanchez-Sanchez, M.; Orcajo, M.G., *Langmuir*, **2010**, *26*, 5300 - 5303.
36. Jee, B.; Eisinger, K.; Gul-E-Noor, F.; Bertmer, M.; Hartmann, M.; Himsl, D.; Poppl, *A., J. Phys. Chem. C.* **2010**, *114*, 16630-16639.
37. Furukawa, S.; Hirai, K.; Nakagawa, K.; Takashima, Y.; Matsuda, R.; Tsuruoka, T.; Kondo, M.; Haruki, R.; Tanaka, D.; Sakamoto, H.; Shimomura, S.; Sakata, O.; Kitagawa, S., *Angew. Chem. Int. Ed.* **2009**, *48*, 1766-1770.
38. (a) Li, J.-R.; Sculley, J.; Zhou, H.-C., *Chem. Rev*. **2012**, *112*, 869. (b) Ma, S.; Zhou, H.-C. *Chem. Commun*. **2010**, *46*, 44. (c) Sculley, J.; Yuan, D.; Zhou, H.-C. *Energy Environ. Sci*., **2011**, *4*, 2721. (d) Murray, L. J.; Dinca, M.; Long, J. R., *Chem. Soc. Rev.* **2009**, *38*, 1294. (e) Rowsell, J. L. C.; Yaghi, O. M. Angew., *Chem., Int. Ed*. **2005***, 44*, 4670.
39. (a) Huxford, R. C.; Della Rocca, J.; Lin, W. B., *Curr. Opin. Chem.Biol*. **2010**, *14*, 262. (b) Della Rocca, J.; Liu, D. M.; Lin, W. B. Acc., *Chem. Res*. **2011**, *44*, 957. (c) Horcajada, P.; Gref, R.; Baati, T.; Allan, P. K.; Maurin, G.; Couvreur, P.; Ferey, G.; Morris, R. E.; Serre, C., *Chem. Rev.* **2012**, *112*, 1232.
40. (a) Lee, J.; Farha, O. K.; Roberts, J.; Scheidt, K. A.; Nguyen, S. T.; Hupp, J. T., *Chem. Soc. Rev*. **2009**, *38*, 1450. (b) Farrusseng, D.; Aguado, S.; Pinel, C., Angew *Chem., Int. Ed*. **2009**, *48*, 7502. (c) Corma, A.; García, H.; Llabre s i Xamena, F. X., *Chem. Rev*. **2010**, *11*0, 4606.
41. (a) Rocha, J.; Carlos, L. D.; Almeida Paz, F. A.; Ananias, D., *Chem. Soc. Rev*. **2011**, *40*, 926. (b) Allendorf, M. D.; Bauer, C. A.; Bhakta, R. K.; Houk, R. J. T., *Chem. Soc. Rev*. **2009**, *38*, 1330.
42. Chen, B.; Xiang, S.; Qian, G. Acc., *Chem. Res*. **2010**, *43*, 1115.
43. (a) Yoon, M.; Suh, K.; Natarajan, S.; Kim, K. Angew., *Chem., Int. Ed*. **2013**, *5*2, 2688. (b) Givaja, G.; Amo-Ochoa, P.; Gomez-Garcia, C. J.; Zamora, F., *Chem. Soc. Rev.* **2012**, *41*, 115. (c) Horike, S.; Umeyama, D.; Kitagawa, S., *Acc. Chem. Res*. **2013**.

44. Yamaguchi, M.; Tanimoto, Y.; Magneto-science, Magnetic field effects on materials : fundamentals and applications, Kodansha & Springer, **2006**.
45. Krishna. R.; Jasper M. van Baten, J., *Membrane Science*, **2010**, *360*, 323-333.
46. Kondo, M; Yoshitomi, T.; Seki, K.; Matsuzaka, H.; Kitagawa, S., *Angew. Chem. Int. Ed.* **1997**, *33*, 1735.
47. Shimomura, S.; Horike, S.; Matsuda, R.; Kitagawa, S., *Chem. Soc*. **2007**, *129*, 10990.
48. Li, W.; Jia, H. P.; Ju, Z.; Zhang, *J., Crystal Growth & Design*. **2006**, Vol. 6 ,No. 9, 2136.
49. Garcia-Ricard, O. J.; Morales, P. M.; Martinez, J. C. S.; Curet-Arana, M. C. ; Hogan, J. A.; Hernandez-Maldonado, A. J., *Microporous and Mesoporous Materials*. **2013**, *177*, 54.
50. Millward; A. R.; Yaghi, O. M.*, J. Am. Chem. Soc*. **2005**, *127*, 17998.
51. Vaidhyanathan, R.; Iremonger, S. S.; Dawson, K. W.; Shimizu, G. K. H, *Chem. Commun.* **2009**, 5230.
52. Lin, L. C.; Kim, J.; Kong, X.; Scott, E.; McDonald, T. M.; Long, J. R.; Reimer, J.A.; Smit, B., *Angew. Chem. Int. Ed.* **2013**, *52*, 4410.
53. Li, J. R.; Ma, Y.; McCarthy, M. C.; Scullay, J.; Yu, J.; Jeong, H. K.; Balbuena, P. B.; Zhou, H. C., *Coord. Chem. Rev*. **2011**, *255*, 1791.
54. Zhai, Q. G.; Hu, M. C.; Li, S. N.; Jiang, Y. C., *Inorganic Chemistry Communications.* **2008**, *11*, 1147.
55. Noro, S.; Kitagawa, S.; Akutagawa,; T.; Nakamura, T., *Prog. Polym. Sci*. **2009**, *34*, 240.
56. Cai, Y.; Zhang, Y.; Huang, Y.; Marder, S. R.; Walton, K. S., *Cryst. Growth De*s. **2012**, *12*, 3709.
57. Onishi, S.; Ohmori, T.; Ohkubo, T.; Noguchi, H.; Hanzawa, L. D. Y.; Kanoh, H.; Kaneko, K., *Applied Surface Scien*ce. **2002**, *196* , 81.
58. Izumi, F.; Momma, K., "Three-dimensional visualization in powder diffraction," Solid State Phenom. **2007**, 130, 15.
59. Izumi, F.; Momma, K., "a Three-dimensional visualization system for electronic and structural analysis, **2014.**

60. Hangx, S. J. T., CATO Work Package WP.4.1. HPT. Laboratory, Department of Earth Sciences Utrecht University, **2005**.
61. Li, H.; Eddaoudi, M.; Groy, T. L.; Yaghi, O. M., *J. Am. Chem. Soc*. **1998**, *120*, 8571.
62. Zhang, C.; Zhang, M.; Qin, L. Zheng, H., *Cryst. Growth Des*. **2014**, *14*, 491.
63. Ariga, K.; Yamauchi, Y.; Rydzek, G.; Ji, Q.; Yonamine, Y.; Wu, K. C. W.; Hill, *J. P., Chem. Lett.* **2014**, *43*, 36–68.
64. Malgras, V.; Ji, Q. Kamachi, Y.; Mori, T.; Shieh, F. K.; Wu, K.C.W.; Ariga, K. ; Yamauchi. Y., *Bull. Chem. Soc. Jpn*. **2015**, 1171.
65. Jikikagaku (Magneto-Science), ed. by Ozeki, S.; Tanimoto, Y.; Yamaguchi, M.; Kitazawa K. (supervised), IPC, Tokyo, **2002** (in Japanese).
66. Magneto-Science, ed. by M. Yamaguchi, Y. Tanimoto, Kodansha-Springer, Tokyo, **2006**.
67. Ozeki, S.; Kurashima, H.; Abe, H., *J. Phys. Chem. B*. **2000**, *104*, 5657.
68. Saravanan, G.; Ozeki S., *J. Phys. Chem. B*. **2008**, *3*,112,
69. Ozeki S. ; Otsuka, I., *J. Phys. Chem. B.* **2006,** *110*, 20067.
70. Otsuka I.; Ozeki, S., *J. Phys. Chem. B*. **2006,** *110*, 1509.
71. A. Banerjee, S. Nandi, P. Nasa, R. Vaidhyanathan, *Chem. Commun*. **2016**, *52*, 1851
72. M. Zubir, A. Hamasaki, T. Iiyama, A. Ohta, H. Ohki, and S. Ozeki, *Chem. Lett*. **2016**, *45*, 362.
73. A. Sakaguchi, A. Hamasaki, T. Sadatou, Y. Nishihara, S. Yamamoto, Y. Sekinuma, S. Ozeki, *Chem. Lett*. **2012,** *12*, 1576.
74. F. Izumi, and K. Momma, "a Three-dimensional visualization system for electronic and structural analysis, **2014**.
75. S. J. Gregg, K. S. W. Sing, Adsorption, Surface Area and Porosity, 2nd ed. Academic Press, London, **1982**.
76. Spek, A. L. Structure validation in chemical crystallography, Acta Cryst., D65, 148-155, **2009.**
77. Hangx, S. J. T.; CATO Work Package WP.4.1. HPT. Laboratory, Department of Earth Sciences Utrecht University. **2005**.
78. Sum, A. K.; Burruss, R. C.; Sloan, E. D. Jr. Measurement of Clathrate Hydrates via Raman Spectroscopy. *J. Phys. Chem. B*, *101*, 7371-7377, **1997**.
79. Sloan, E. D. Jr.; Koh, C. A. "Clathrate Hydrates of Natural Gases", 3rd. Ed., CRC

Press, **2008**.

80. Kitaura, R.; Kitagawa, S.; Kubota, Y.: Kobayashi, T. C.; Kindo, K.; Mita, Y.; Matsuo, A.; Kobayashi, M.; Chang, H.-C.; Ozawa, T. C.; Suzuki, M.; Sakata, M.; Takata, M. *Science*, **2002,** *298*, 2358-2361.
81. Urita, K.; Shiga, Y.; Fujimori, T.; Iiyama, T.; Hattori, Y.; Kanoh, H.: Ohba, T.; Tanaka, H.; Yudasaka, M.; Iijima, S.; Moriguchi, I.; Okino, F.; Endo, M.; Kaneko, K. , *J. Am. Chem. Soc*., **2011,** *133*, 10344-10347.
82. Fujimori, T.; Morelos-Gómez, A.; Zhu, Z.; Muramatsu, H.; Futamura, R., Urita, K.; Terrones, M.; Hayashi, T., Endo, M.; Hong, S. Y.; Choi, Y. C.; Tománek, D.; Kaneko, K. , *Nature Commun*., **2013,** *4*, 2162-2169.
83. Imai, J.; Souma, M.; Ozeki, S.; Suzuki, T.; Kaneko, K., *J. Phys. Chem*., *95*, 9955-9960, **1991**.

ACKNOWLEDGEMENTS

Foremost, I would like to express my sincere gratitude to my supervisor, Prof. Sumio Ozeki to the continuous support of my Ph.D study and research, for his patient, motivation, enthusiasm, and immense knowledge. I am grateful for his generous guidance and support made it possible for me to work on a topic that was of great interest to me. His guidance helped me in all the time of research and writing of this thesis and my papers. It was a pleasure working with him.

Beside my supervisor, I am grateful to my co-supervisor, Prof. Taku Iiyama for adsorption knowledge and supporting my research and also to Prof. Hiroshi Ohki for Rietveld analysis to built the crystal structure of my experiment. I am highly indebted for their encouragement, insightful comments, and hard question. I am grateful also to Prof. Akira Ohta form Organic Chemistry Laboratory of Shinshu University for his strong support of elemental analysis and his guidance to the elemental analysis technique and organic ligands reaction analysis.

My sincere thanks also goes to Dr. Atom Hamasaki for his strongly technical support during my research and especially his support to prepare adsorption isotherms equipment system and data analysis and also for IR analysis which very helpful to make my second paper accepted. Also for his kindness to his guidance for TG/DTA analysis in Shinshu University Nagano Campus.

My thankful To Mr. Hayato Otsuka for his support for IR analysis and also during preparation for my final examination. His good English many helped me to prepare many document for university and helping me shape up my Japanese translation skill.

I would like thankful also to all my tutor during 3 years, Mr. Masato Ogusu, Mr. Jin Uchimura and Mr. Kaida Keichiro for their supporting and motivation for my daily life settle in Japan

and also preparation of my experiment. And also thankful to all physical chemistry students during 4 years, both of magnetic group and also adsorption group. Thank you to help me understand from the Japanese to English and also their kindness during the hard working experiment in physical chemistry laboratory in Shinshu University.

I would like to express my gratitude to Prof. Edison Munaf and Prof. Rahmiana Zein from Andalas University, Padang-West Sumatera, Indonesia, for his motivation to me and others Andalas University student to study in Japan or others abroad university to improve our knowledge for our next future in Indonesia. Also I am grateful to Prof. Jiye Jin in Analytical Chemistry Laboratory of Shinshu University for his kindness corporation for Andalas University student can continue our study in Shinshu University Japan.

I would like to express my gratitude also to Rector of State University of Medan, Prof. Ibnu Hajar Damanik and Prof. Syawal Gultom to their approval of continue and finish my doctoral course after I was accepted as Lecturer at State University of Medan on April 2014. Their strong supports have motivated me to finish my doctoral course soon and then can start to working as lecturer in our institution.

I would like to thankful to Ministry of Education, Culture, Sports, Science and Technology (MEXT / MONBUKAGAKUSHO) – Japan, that have supported my doctoral course scholarship in Shinshu University, Matsumoto, Japan for 3,5 years.

Last but not the least, my deep gratitude to all my teachers in Andalas University, Padang, West Sumatera , Indonesia and also in Shinshu University, Matsumoto, Japan who put their faith in me and urged me to be better. And also my grateful to my family : my parents and my wife, for giving birth to me at the first place and supporting me spiritually throughout my life.

Publication List

1. Moondra Zubir, Atom Hamasaki, Taku Iiyama, Akira Ohta, Hiroshi Ohki, Sumio Ozeki, "Magnetic Field Control of Micropore Formation in $[Zn_2(Oxac)(Taz)_2].(H_2O)_x$", Chemistry Letters, 2016, **45**, 362.

2. Moondra Zubir, Atom Hamasaki, Taku Iiyama, Akira Ohta, Hiroshi Ohki, Sumio Ozeki, "Micropore Formation of $[Zn_2(Oxac)(Taz)_2]\bullet(H_2O)_{2.5}$ via CO_2 adsorption", Langmuir 2017, **33**, 680-684.

Conference List

1. International Conference on Magneto Science, held on October 13th-17th, 2013 at Bordeaux, France. **"Magnetic Field Control of Structure and Gas Adsorptivity of Organometallic Complexes".**
   Moondra Zubir, Koichi Hashikawa, Atom Hamasaki, and Sumio Ozeki.

2. The 65th Divisional Meeting on Colloid and Surface Chemistry, the Chemical Society of Japan, held on September 3rd – 5th, 2014 at Tokyo University of Science, Tokyo - Japan. **"Pore Structure of Amine-Functionalized Porous Coordination Polymers".**
   Moondra Zubir, Atom Hamasaki, and Sumio Ozeki.

3. The 9th Annual Meeting of the Magneto Science Society of Japan, held on November 13th-14th , 2014 at Takayama, Japan. **" Magnetic field control of structure and gas adsorptivity of the porous coordination polymers of Zn/triazole/oxalic acid ".**
   Moondra Zubir, Atom Hamasaki, and Sumio Ozeki.

4. The 95th Annual Meeting The Chemical Society of Japan, held on March 26th – 29th, 2015 at Nihon University, Chiba – Japan. **"Magnetic field effects on crystal structures and pore properties of porous coordination polymers of Zn/triazole/oxalic acid".**
   Moondra Zubir, Atom Hamasaki, and Sumio Ozeki.

5. International Conference on Magneto Science, held on October 27th-31th , 2013 at Matsumoto, Japan. **"Magnetic field effects on pore properties of porous coordination polymers comprising Zn^{2+}, Triazole and oxalic acid."**
   Moondra Zubir, Atom Hamasaki, Hiroshi Ohki, and Sumio Ozeki.